ประสิทธิภาพของโอเซลทามิเวียร์ต่อนิวรามินิเดสของไวรัสไข้หวัดใหญ่ชนิดบีกลายพันธุ์โดยการจำลองพลวัตเชิงโมเลกุล

นางสาวจิราพร  เต็งรัง

วิทยานิพนธ์นี้เป็นส่วนหนึ่งของการศึกษาตามหลักสูตรปริญญาวิทยาศาสตรมหาบัณฑิต
สาขาวิชาเคมี  ภาควิชาเคมี
คณะวิทยาศาสตร์  จุฬาลงกรณ์มหาวิทยาลัย
ปีการศึกษา  2554

OSELTAMIVIR EFFICIENCY TOWARD NEURAMINIDASE OF MUTANT STRAINS OF

INFLUENZA B VIRUS USING MOLECULAR DYNAMICS SIMULATIONS

Miss Jiraporn   Tengrang

A Thesis Submitted in Partial Fulfillment of the Requirements

for the Degree of Master of Science Program in Chemistry

Department of Chemistry

Faculty of Science

Chulalongkorn University

Academic Year 2011

Thesis Title         OSELTAMIVIR EFFICIENCY TOWARD NEURAMINIDASE OF
                     MUTANT STRAINS OF INFLUENZA B VIRUS USING
                     MOLECULAR DYNAMICS SIMULATIONS
By                   Miss Jiraporn Tengrang
Field of Study       Chemistry
Thesis Advisor       Professor Supot Hannongbua, Dr.rer.nat.
Thesis Co-advisor    Thanyada Rungrotmongkol, Ph.D.

Accepted by the Faculty of Science, Chulalongkorn University in Partial Fulfillment of the Requirements for the Master's Degree

………………….……………………….. Dean of the Faculty of Science

(Professor Supot Hannongbua, Dr.rer.nat.)

THESIS COMMITTEE

………………….……………………….. Chairman

(Assistant Professor Warinthorn Chavasiri, Ph.D.)

………………….……………………..……. Thesis Advisor

(Professor Supot Hannongbua, Dr.rer.nat.)

………………….……………………….. Thesis Co-advisor

(Thanyada Rungrotmongkol, Ph.D.)

………………….……………………….. Examiner

(Associate Professor Polkit Sangvanich, Ph.D.)

………………….……………………….. External Examiner

(Nadtanet Nunthaboot, Ph.D.)

จิราพร เต็งรัง : ประสิทธิภาพของโอเซลทามิเวียร์ต่อนิวรามินิเดสของไวรัสไข้หวัด
ใหญ่ชนิดบีกลายพันธุ์โดยการจำลองพลวัตเชิงโมเลกุล. (OSELTAMIVIR
EFFICIENCY TOWARD NEURAMINIDASE OF MUTANT STRAINS OF
INFLUENZA B VIRUS USING MOLECULAR DYNAMICS SIMULATIONS) อ. ที่
ปรึกษาวิทยานิพนธ์หลัก : ศ.ดร. สุพจน์ หารหนองบัว, อ. ที่ปรึกษาวิทยานิพนธ์ร่วม :
อ.ดร. ธัญญดา รุ่งโรจน์มงคล, 51 หน้า.

ไวรัสไข้หวัดใหญ่ชนิดบีเป็นสาเหตุของโรคไข้หวัดใหญ่ตามฤดูกาลที่ระบาดหนักใน
ทุกๆ 2-3 ปี ทำให้เกิดการเจ็บป่วยในคนเป็นจำนวนมาก ยาโอเซลทามิเวียร์เป็นยาที่สามารถ
รักษาการติดเชื้อไวรัสไข้หวัดใหญ่ชนิดบีได้โดยยับยั้งการทำงานของเอนไซม์นิวรามินิเดส
(NA) เพื่อป้องกันการแพร่กระจายของไวรัสตัวใหม่ อย่างไรก็ตามพบว่า มีการดื้อยาอันเกิดจาก
การกลายพันธุ์ของเอนไซม์นิวรามินิเดสที่ตำแหน่ง E119G, R152K และ D198N เกิดขึ้น
งานวิจัยนี้ได้ศึกษาการจำลองพลวัตเชิงโมเลกุลของสารประกอบระหว่างเอนไซม์นิวรามินิเดส
ทั้งในสายพันธุ์ดั้งเดิมและสายพันธุ์ที่กลายพันธุ์ข้างต้นกับยาโอเซลทามิเวียร์ จากการจำลอง
ระบบเป็นจำนวนสามซ้ำ พบว่า สายพันธุ์ดั้งเดิมจับกับยาโอเซลทามิเวียร์ได้ดีที่สุดโดยเกิด
พันธะที่แข็งแรงกับกรดอะมิโนที่สำคัญ 5 ตำแหน่ง คือ E119, D151, R152, R292 และ R371
การสูญเสียพันธะไฮโดรเจนและการลดลงของค่าพลังงานอิสระของการยึดจับของแต่ละ
กรดอะมิโนที่ตำแหน่งกลายพันธุ์ G119 และ K152 เมื่อเทียบกับสายพันธุ์ดั้งเดิม เป็นสาเหตุ
หลักของการดื้อยาโอเซลทามิเวียร์ในปริมาณสูงของสายพันธุ์ E119G และ R152K นอกจากนี้
โพรงของนิวรามินิเดสที่มีขนาดใหญ่ขึ้นรอบๆ หมู่ฟังก์ชัน –NH$_3^+$ และ –NHAc ของโอเซลทามิ
เวียร์ อันเกิดจากการกลายพันธุ์ของสองสายพันธุ์ข้างต้นตามลำดับ ยังทำให้โมเลกุลของน้ำ
แทรกเข้ามาจับกับยาแทน ในทางตรงกันข้ามสายพันธุ์ D198N ดื้อยาในปริมาณต่ำ เนื่องจาก
พันธะไฮโดรเจนที่ยึดจับระหว่างยากับนิวรามินิเดสสายพันธุ์นี้ลดลงเพียงเล็กน้อยเท่านั้น จาก
การคำนวณค่าพลังงานอิสระของการยึดจับระหว่างยาโอเซลทามิเวียร์กับนิวรามินิเดสด้วยวิธี
MM/PBSA พบว่า ประสิทธิภาพการออกฤทธิ์ของโอเซลทามิเวียร์สามารถเรียงลำดับได้ดังนี้
คือ wild-type> D198N > E119G> R152K ซึ่งสอดคล้องกับผลการทดลอง

| ภาควิชา | เคมี | ลายมือชื่อนิสิต |
|---|---|---|
| สาขาวิชา | เคมี | ลายมือชื่อ อ.ที่ปรึกษาวิทยานิพนธ์หลัก |
| ปีการศึกษา | 2554 | ลายมือชื่อ อ.ที่ปรึกษาวิทยานิพนธ์ร่วม |

# # 5272645223 : MAJOR  CHEMISTRY

KEYWORDS :INFLUENZA B VIRUS/ NEURAMINIDASE/ OSELTAMIVIR RESISTANCE / MOLECULAR DYNAMICS SIMULATION

JIRAPORN  TENGRANG  :  OSELTAMIVIR  EFFICIENCY  TOWARD NEURAMINIDASE OF MUTANT STRAINS OF INFLUENZA B VIRUS USING MOLECULAR  DYNAMICS  SIMULATIONS.  ADVISOR  :  PROF.  SUPOT HANNONGBUA,  Dr.rer.nat.,  CO-ADVISOR  :  THANYADA RUNGROTMONGKOL, Ph.D., 51 pp.

The influenza B virus causes epidemics of influenza in every 2-3 years serving high morbidity in humans. Oseltamivir, the neuraminidase (NA) inhibitor blocking the releasing of new viruses, is an effective agent against influenza B virus, however, the oseltamivir resistances conferring the E119G, R152K and D198N substitutions have been reported. In this study, molecular dynamics (MD) simulation was performed on the wild-type and the three NA mutants with oseltamivir bound. Based on three different of MD simulations, the wild-type system is the most stability which oseltamivir strongly binds through the five key residues E119, D151, R152, R292 and R371. The notable loss of hydrogen bond and the decrease in per-residue decomposition energy at the mutated residues G119 and K152 compared to those of the wild-type were found to be the primary source of high-level oseltamivir resistance in the E119G and R152K mutants, respectively. In addition, the larger cavities in the NA active site conferring with these two mutations at the $-NH_3^+$ and $-NHAc$ side chains, respectively, were compensated by more accessibility of water molecules. In contrast to the low level oseltamvir resistance in D198N mutant, this strain only showed slightly decreased in hydrogen bonds. According to the MM/PBSA binding free energies, the order of oseltamivir efficiency is of wild-type > D198N > E119G > R152K in good agreement with the experimental $IC_{50}$ values.

Department : Chemistry ............................  Student's Signature Jiraporn Te...........

Field of Study : Chemistry ......................  Advisor's Signature S. Hannongbua

Academic Year : 2011 ...........................  Co-advisor's Signature T Rungrotmongkol

# ACKNOWLEDGEMENTS

# CONTENTS

# LIST OF TABLES

# LIST OF FIGURES

# LIST OF ABBREVIATIONS

| | | |
|---|---|---|
| 3D | = | Three dimension |
| 3D-RISM | = | Three dimension reference interaction site model |
| 3-site | = | Three-site |
| Ala(A) | = | Alanine |
| Arg (R) | = | Arginine |
| Asn (N) | = | Asparagine |
| Asp (D) | = | Aspatic acid |
| Ele | = | Electrostatic |
| GB | = | Generalized Born |
| GISRS | = | Global influenza surveillance and response system |
| Gln (Q) | = | Glutamine |
| Glu (E) | = | Glutamic Acid |
| Gly (G) | = | Glycine |
| HA | = | Hemagglutinin |
| His (H) | = | Histidine |
| $IC_{50}$ | = | Median Inhibition Concentration  that reduces the effect by 50% |
| Ile (I) | = | Isoleucine |
| KH | = | Kovalenko-Hirata closure relation |
| L-J | = | Lennard-Jones potential |

Lys (K)      = Lysine

M2      = Matrix protein 2

MD      = Molecular Dynamics

MM/GBSA      = Molecular Mechanic/Generalized-Born Surface Area

MM/PBSA      = Molecular Mechanic/Poisson-Boltzmann Surface Area

MOZ      = Molecular Ornstein - Zernike

NA      = Neuraminidase

NAI      = Neuraminidase inhibitor

NP      = Nucleocapsid protein

NS      = Non-structural protein

PA      = Polymerase A protein

PB      = Poisson Boltzmann

PB1      = Polymerase B1 protein

PB2      = Polymerase B2 protein

PDB      = Protein Data Bank

pH1N1      = Pandemic of influenza A(H1N1)

PME      = Particle-mesh Ewald

RDF      = Radial Distribution Functions

RESP      = Restrained electrostatic potential

RMSD      = Root Mean Square Deviation

RNA     =   Ribonucleic acid

SASA     =   Solvent Accessible Surface Area

Ser (S)     =   Serine

TIP3P     =   Transferable intermolecular potential three -position

Trp (W)     =   Tryptophan

Tyr (Y)     =   Tyrosine

Val (V)     =   Valine

vdW     =   van der Waals

WHO     =   World Health Organization

# CHAPTER I

# Introduction

## 1.1 The seasonal influenza

Each year the annual influenza epidemics caused by influenza A and B viruses are related with a quarter to half a million deaths worldwide [WHO, 2009 : online]. Although influenza B viruses do not have a pandemic potential like influenza A viruses that mainly cause significant morbidity and mortality in humans, but influenza B viruses are the predominant circulating virus that serves illness in every 2-3 years [Lin et al., 2004; Jackson, Elderfield, and Barclay, 2011]. The last wave occurs at the early 2011 which analyzed belong to the lineage of B/Victoria, B/Yamagata and B/not determined [WHO, 2011: online].
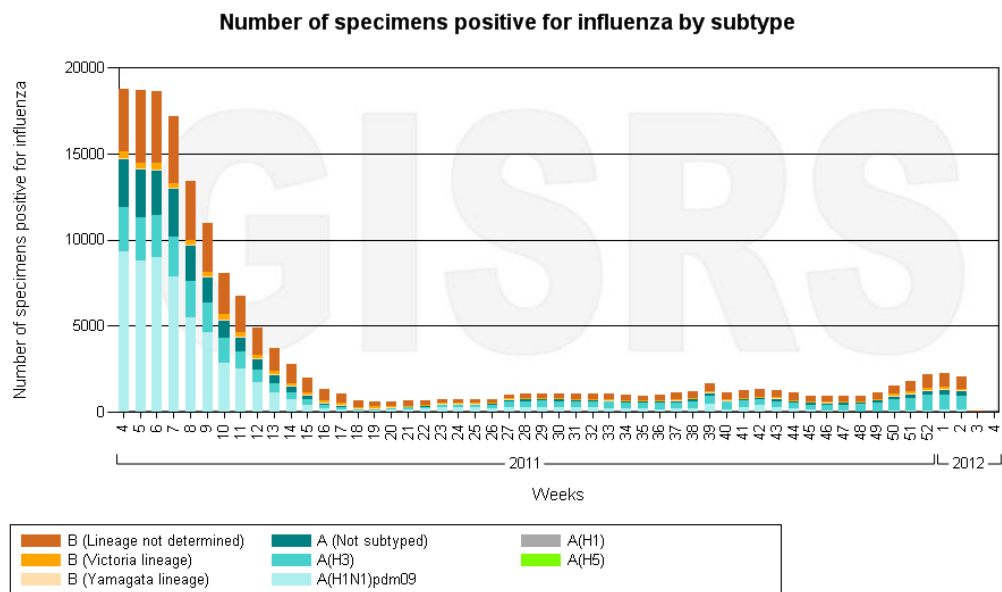


**Figure 1.1** The global circulation of seasonal influenza viruses in 2011 observed by Global influenza surveillance and response system (GISRS) [WHO, 2011: online].

For the situation in Thailand, the predominant circulating of influenza B viruses were detected the peak at the late of 2011 with the lineage spread of B/Victoria and B/not determined. The influenza A(H1N1), A(H3N2) and B viruses have circulated among humans, therefore, they were included in the seasonal

influenza vaccine for the upcoming season, the primary strategy to prevent the infection of influenza [Barr et al., 2010].
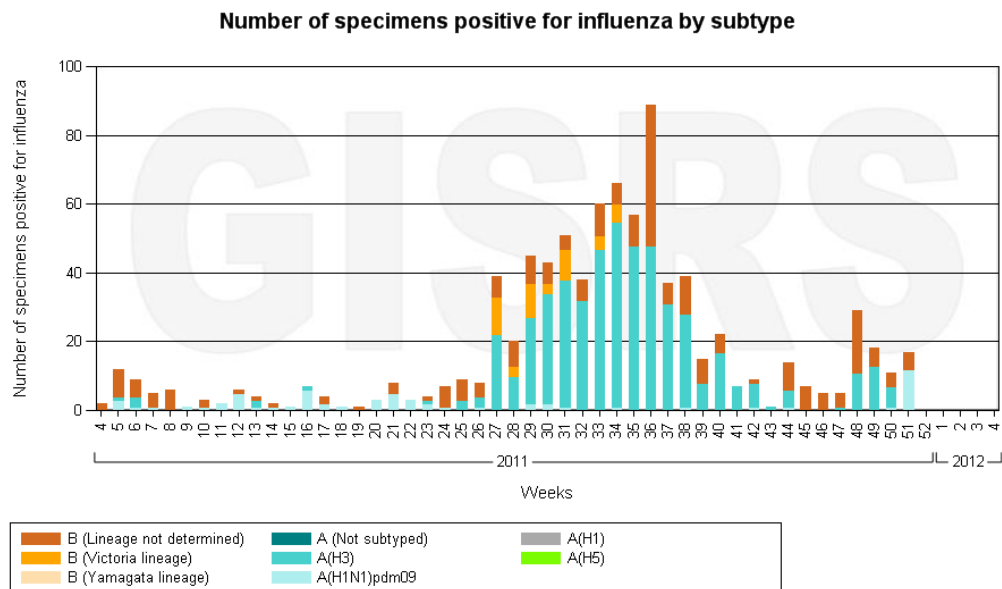


**Figure 1.2** The 2011 situation of seasonal influenza viruses in Thailand monitoring by GISRS [WHO, 2011: online].

Therefore, the circulation of influenza B virus is important and cannot ignore. The experimental and theoretical studies of influenza B virus are considerably less than those of influenza A virus which leads to the main goal of the present work in understanding the drug inhibition toward influenza B virus.

## 1.2 Influenza B virus

Influenza B virus is one of the three distinct influenza virus types that was isolated by Francis in 1939 [Francis, 1940]. All three types share many features and viral activities (Table 1.1), however, the influenza B virus habours an unique genetic and can infect only humans [Wright and Webster, 2001; Gürtler 2006; Treanor, 2010]. The influenza B virus consists of eight gene segments, polymerase B2 protein (PB2), polymerase B1 protein (PB1), polymerase A protein (PA), hemagglutinin (HA), nucleocapsid protein (NP), neuraminidase (NA), matrix protein (M2) and non-

structural protein (NS), which encode 11 viral proteins. However, two proteins, NB and BM2 of influenza B are unique [Hatta and Kawaoka, 2003].

**Table 1.1** The differences among three types of influenza viruses

|  | Influenza A | Influenza B | Influenza C |
|---|---|---|---|
| Genomes | 8 gene segments | 8 gene segments | 7 gene segments |
| Structure | 10 viral proteins with unique M2 | 11 viral proteins with unique NB | 9 viral proteins with unique HEF |
| Natural host | Humans,swine, equine, avian, marine mammals | Humans only | Humans and swine |
| Clinical presentation | May cause large pandemics with significant mortality in young persons | Severe disease generally confined to older adults or persons at high risk | Mild disease without seasonality |

Both of influenza A and B viruses have three important proteins on their surface membrane, HA, NA and M2 channel. As seen in Fig. 1.3, HA attaches to the sialic acid via the carbohydrate side chains of cell surface glycoproteins and glycolipids for entry into the host cell. Consequently, the M2 protein acts as an ion channel pump allowing proton transfer. Following virus replication, the receptor destroying enzyme, NA, removes its substrate from the infected cell in order to infect new cells.
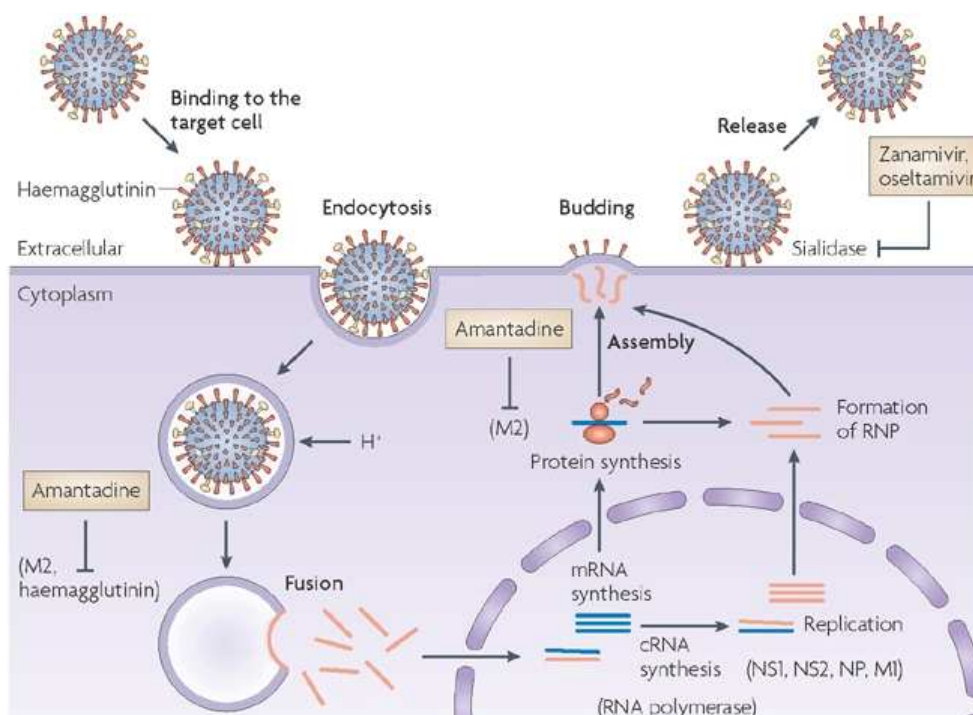
**Figure 1.3** The influenza virus life cycle is divided as the following stages, the penetration into host cell; transcription and replication of viral RNA; assembly and budding of virion; releasing of new viruses from host cell, while the target for antiviral agents also shown (von Itzstein, 2007).

There are two groups of anti-influenza agents, M2 inhibitors and NA inhibitors (NAI). The M2 inhibitors (amantadine and rimantadine) which target the influenza A M2 protein, are ineffective against influenza B virus. This is because the M2 of influenza B appears the polar residues which reduce the accommodation for hydrophobic adamantane moiety of the M2 inhibitors [Pinto and Lamb, 2006].

Interesting, the NAIs (zanamivir, oseltamivir, peramivir and laninamivir) have been shown to be effective against both influenza A and B types, as the active site residues of NAs among them are highly conserved [Gubareva, Kaiser, and Hayden, 2000; McKimm-Breschkin 2002; Ward et al., 2005; Yamashita et al., 2009]. Hence, the surface glycoprotein NA has been served as the important target for drug design and development against influenza.

### 1.2.1 Neuraminidase

Neuraminidase (NA) acts as an enzyme, cleaving sialic acid from the HA molecule, from other NA molecules and from glycoproteins and glycolipids at the cell surface and seems to be necessary for the penetration of the virus through the mucin layer of the respiratory epithelium. The tetrameric NA of the influenza virus was classified in three distinct groups, including group-1 and group-2 NA of influenza A plus the different influenza B NA [Russell et al., 2006]. The available crystal structures of influenza B NA are from B/Beijing/1/87 [Burmeister, 1993], B/Lee/40 [Janakiraman, 1994] and B/Perth/211/2001 [Oakley, 2010] that show the closed form of 150-loop, the tight conformation of residues 147-152 (N2 numbering) from the active site. Based on sequence alignment of NA residues at the binding pocket, all residues in the catalytic (bold) and framework (regular) sites are highly conserved among influenza A and B viruses, whereas the difference is found at two residues nearby framework site (underline), residue numbers 347 and 405, as summarized in Table 1.2. However, the genetic and structural relationship between influenza A and B are significant difference as can be seen by the percentage of sequence identity and similarity as well as RMSD values in Table 1.3.

**Table 1.2** The sequence alignment of NA catalytic sites, framework sites and nearby framework sites between influenza A viruses and influenza B virus

| N2 numbering | **118** | 119 | **151** | **152** | 156 | 178 | 179 | 198 | 222 | **224** | 227 | 274 | **276** | 277 | **292** | 294 | 347 | **371** | 405 | 406 | 425 |
|---|---|---|---|---|---|---|---|---|---|---|---|---|---|---|---|---|---|---|---|---|---|
| B/Beijing[a] | **R** | E | **D** | **R** | R | W | S | D | I | **R** | E | H | **E** | E | **R** | N | G | **R** | W | Y | E |
| A/pH1N1[b] | **R** | E | **D** | **R** | R | W | S | D | I | **R** | E | H | **E** | E | **R** | N | N | **R** | G | Y | E |
| A/H5N1[c] | **R** | E | **D** | **R** | R | W | S | D | I | **R** | E | H | **E** | E | **R** | N | Y | **R** | G | Y | E |
| A/H2N2[d] | **R** | E | **D** | **R** | R | W | S | D | I | **R** | E | H | **E** | E | **R** | N | Q | **R** | G | Y | E |

[a] B/Beijing/1/87 strain, 1NSC.pdb [Burmeister et al., 1993]

[b] A/California/4/2009 strain, 3TI6.pdb [Vavricka et al., 2011]

[c] A/Vietnam/1203 strain, 2HU4.pdb [Russell et al., 2006]

[d] A/Tokyo/3/1967 strain, 2BAT.pdb [Varghese et al., 1992]

**Table 1.3** The genetic and structural relationship between influenza A and influenza
B viruses

| Influenza B | pH1N1 | H5N1 | H2N2 |
|---|---|---|---|
| %Sequence identity | 34 | 33 | 31 |
| %Sequence similarity | 54 | 53 | 49 |
| RMSD (Å) | 2.3 | 2.3 | 2.3 |

### 1.2.2 Neuraminidase inhibitors

Up to date, the available NAIs are zanamivir, oseltamivir, peramivir and laninamivir, as their chemical structure was presented in Fig. 1.4. Zanamivir (Relenza® marketed by GlaxoSmithKline), the first commercial NAI, is administered by inhalation and recently developed in Phase III trial for intravenous antiviral, while an oral drug oseltamivir (Tamiflu® from Roche) has been used for treatment the influenza A and B viruses. The intravenous peramivir is an unapproved investigational NAI and is still being evaluated in phase III of clinical trials, which was instantly authorized for treatment the pandemic influenza H1N1 in 2009 [Birnkrant and Cox, 2009]. Recently, laninamivir was approved and marketed in 2010, however, its efficiency against influenza B virus is lower than either zanamivir or oseltamivir [Yamashita et al., 2009].

According to data from marketing research media between 2008-2009, the annual production of oral drug oseltamivir is approximately 5-6 times to zanamivir [Marketing research media, data on file], suggesting that oseltamivir is often used rather than zanamivir which is administered by inhalation. However, high amount of oseltamivir treatment has rapidly caused the mutation of NA gene resulted in resistance to NAIs [Suguya et al., 2007].
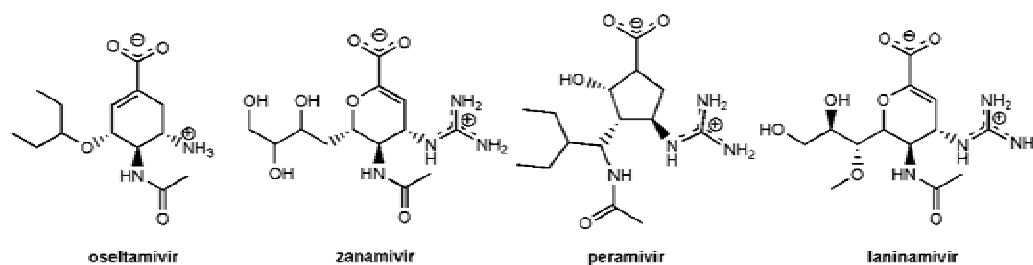
**Figure 1.4** The chemical structures of the four NA inhibitors (NAIs) in active metabolite form, oseltamivir, zanamivir, peramivir and laninamivir [Rungrotmongkol et al., 2011].

## 1.3 Literature reviews on resistance of influenza B NA

Here, The NA mutations which lead to oseltamivir resistance from *in vitro* or *in vivo* experiment and/or isolation from patients both of influenza A and B viruses were listed. The seasonal influenza H1N1 and avian influenza H5N1 viruses carry the single H274Y and N294S substitutions in NA [Le et al., 2005; Yen et al., 2007; Abed et al., 2008; Collins et al., 2008], whereas the pandemic H1N1 2009 (pH1N1) NAs with the single H274Y, I223R and S246N mutants and the S246N and H274Y double mutant are resistant to oseltamivir [Hurt et al., 2011]. In H3N2, the oseltamivir-resistant variants contain the single E119V, R292K and N294S mutations [Kiso et al., 2004]. For influenza B virus, the emergence reduced NAIs sensitivities of E119G, R152K and D198N mutations have been isolated from the patients after drug treatment [Gubareva et al., 1998; Barnett et al., 1999; Gubareva, 2004]. Interestingly, these three important substitutions are not found on NA gene of influenza A viruses.

The susceptibilities of NAI (zanamivir, oseltamivir and peramivir) conferring these substitutions in influenza B virus are listed in Table 1.4. According to oseltamivir was mostly used for treatment the influenza B infection, this research aims to understand the oseltamivir resistance. In *in vivo* study, the R152K and D198N NA mutants have caused the reduction of oseltamivir inhibitory activities with 100- and 9-fold resistances, respectively [Mishin, Hayden, and Gubareva, 2005]. Using reverse genetic, the oseltamivir showed lowered efficiency against R152K and E119G NA strains isolated from the patient after zanamivir treatment with 252- and 31-fold resistances, respectively [Jackson Barclay, and Zürcher 2005].

**Table 1.4** Susceptibility of substitution in influenza B strains and their drug resistance

| Mutant in NA | Susceptibility (fold resistance[a]) | | | Reference |
|---|---|---|---|---|
| | Zanamivir | Oseltamivir | Peramivir | |
| E119G | >560 | 31 | >1,598 | Jackson et al., 2005 |
| | (1.0/>550) | (1.8/57.0) | (0.3/>550) | |
| R152K | 5 | 252 | 214 | Jackson et al., 2005 |
| | (1.0/4.6) | (1.8/462.2) | (0.3/73.8) | |
| | 70 | 100 | 400 | Mishin et al., 2005 |
| | (3.2/220.0) | (4.0/400.0) | (1.0/400.0) | |
| D198N | 9 | 9 | 5 | Mishin et al., 2005 |
| | (1.6/15) | (33/304) | (1.2/5.8) | |

[a] Fold resistance is the ratio of $IC_{50}$ in the mutant and wild-type strains.

**1.4 Scope of this research**

Since no previous study of influenza B NA by molecular modeling, therefore, the molecular dynamic (MD) simulation was carried out to elucidate the drug-target interaction of influenza B NA both wild-type and three important mutations, E119G, R152K and D198N. The basic results at molecular level obtained from our calculation will give the valuable information for structure-based drug design of influenza virus.

There are two objectives for this research.

1. To understand how oseltamivir inhibit influenza B NA

2. To investigate the source of oseltamivir resistance due to the three single substitutions of E119G, R152K and D198N in influenza B NA

# CHAPTER II

# THEORY

## 2.1 Molecular dynamics simulation

Molecular dynamics (MD) simulation is a principal tool in theoretical approach for calculating the time dependent behavior of molecular system at the microscopic level concerning the time dependent calculation [Karplus and McCammon, 2002; Rapaport, 2004]. This technique plays an important role in the study of biological systems such as protein, nucleic acid and their complexes, as it can provide the information of structure, dynamics and thermodynamics properties is often more easier than those obtained from the experiments. In particular, the drug-target interaction obtained from MD simulation is the basic information for designing and developing the new potent inhibitor.

### 2.1.1 Statistical mechanics

MD simulation provides the information at the molecular level (such as energy, intramolecular and intermolecular interactions), including the atomic positions and velocitites. This microscopic information requires statistical mechanics, for converting to the macroscopic observation. Statistical mechanics studies the macroscopic properties from the molecular point of view which is considered as the ensemble averages [McQuarrie, 1976]. Ensemble is the collection of all possible configurations which have different microscopic states but the macroscopic or thermodynamic states are identical.

Because of the sample contains an extremely large number of molecules with a huge number of conformations, the calculating averages from MD simulation are characterized as the ensemble averages. An ensemble average, $\langle A \rangle_{ensemble}$, is an average of the replicas of the simulated system as shown (1) which is extremely difficult to integration over all possible states.

$$\langle A \rangle_{ensemble} = \int\int dp^N dr^N A(p^N, r^N) \rho(p^N, r^N) \tag{1}$$

where $A(p^N, r^N)$ is the observable of interest that is express as the function of the momenta ($p$) and the positions ($r$) of the system. The probability density ($\rho_i$) of the ensemble using the Boltzmann distribution is given by (2).

$$\rho_i = \frac{1}{q}\exp\left(\frac{-\varepsilon_i}{k_B T}\right) \tag{2}$$

where $\varepsilon_i$ is a particular energy level, $k_B$ is the Boltzmann constant and $q$ is the molecular partition function given by the summation of all accessible energy levels in equation (3).

$$q = \sum_i \exp\left(\frac{-\varepsilon_i}{k_B T}\right) \tag{3}$$

On the other hand, MD simulation considered as the time average of ensemble average is expressed as (4).

$$\langle A \rangle_{time} = \lim_{\tau \to \infty} \frac{1}{\tau}\int_{t=0}^{\tau} A(p^N(t), r^N(t)) dt \approx \frac{1}{M}\sum_{t=1}^{M} A(p^N, r^N) \tag{4}$$

where $\tau$ is the simulation time, $M$ is the number of time steps.

However the experimental observation is assumed through the ensemble averages in which the MD simulation calculate by the time average. The problem is solved by the **ergodic hypothesis** which is the important axiom of statistical mechanics. This hypothesis states that the time average equals to the ensemble average.

$$\langle A \rangle_{ensemble} = \langle A \rangle_{time} \quad \text{(ensemble average = time average)} \tag{5}$$

This means that all possible states can be obtained by allowing the system to evolve in time indefinitely. As a result, MD simulation is to generate enough representative conformations such that this equality is satisfied.

### 2.1.2 Classical Mechanics

The molecular dynamics simulation lies on classical mechanics, especially Newton's second law in equation (6).

$$F = ma \tag{6}$$

where $F$ is the force applied on the particle, while $m$ and $a$ are its mass and acceleration, respectively. Basically, the determination of the atom acceleration in the system can be computed from the force on each atom. The integration of the equations of motion yields the positions, velocities and accelerations of the particles as function of time called trajectory. Consequently, the average values of properties can be determined through the trajectories.

The force can also be expressed as the derivation of the potential energy ($U$).

$$F_i = -\nabla_i U \tag{7}$$

To combine the (6) and (7) equations together, the force is related to the acceleration and in turn to the potential energy described by equation (8).

$$F_i = -\nabla_i U = m_i a = m_i \frac{dv_i}{dt} = m_i \frac{d^2 r_i}{d^2 t} \tag{8}$$

In simple case that acceleration is constant, the velocity after integration can be expressed as equation (9). Likewise, the integration of this velocity yields the coordinate as drawn in following equation (10).

$$v = at + v_0 \tag{9}$$

$$r = vt + r_0 \tag{10}$$

As combining these two equations, the value of coordinate ($r$) at the time ($t$) is the function of the acceleration $(a)$, the initial position ($r_0$) and the initial velocity ($v_0$) as written (11).

$$r = at^2 + v_0 t + r_0 \tag{11}$$

Therefore, the trajectory is achieved by solving this equation which only needs the initial positions, velocities and acceleration of the atoms. $r_0$ is obtained from the experimental structure using X-ray or NMR spectroscopy. $v_0$ is dependent on the random number generator and $a$ is calculated by the derivative of the potential energy with respect to the position as given (12).

$$a = -\frac{1}{m}\frac{dU}{dr} \tag{12}$$

### 2.1.3 Potential energy

The potential energy is a sum of bonded and non-bonded interactions concerning as the function of the positions (13). The summation of bonds, angles and dihedrals energies is of the bonded interaction, while the electrostatic and van der Waals energies are the non-bonded interaction (14).

$$U = U_{bonded} + U_{non-bonded} \tag{13}$$

$$U = \left(U_{bonds} + U_{angles} + U_{dihedrals}\right)_{bonded} + \left(U_{ele} + U_{vdW}\right)_{non-bonded} \tag{14}$$
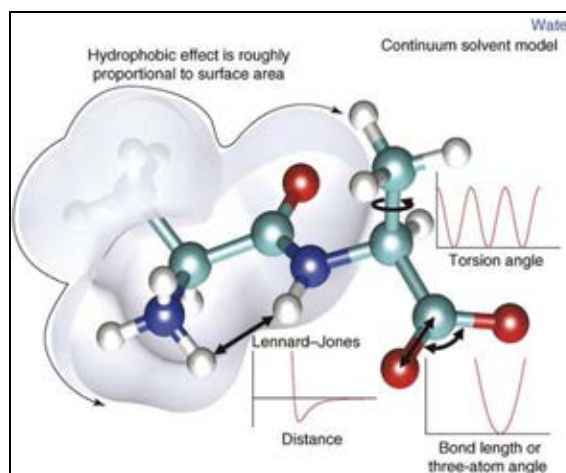


**Figure 2.1** Illustration of potential energy function; bonds, angles and dihedrals energies, as well as van der Waals energy [Boas and Harbury, 2007]

The bonded interaction can be written as following (15).

$$U_{bonded} = \sum_{bonds} k_b (r - r_0)^2 + \sum_{angles} k_\theta (\theta - \theta_0)^2 + \sum_{dihedrals} \frac{V_n}{2} (1 + \cos[n\tau - \phi]) \tag{15}$$

where $k_b$ and $k_\theta$ are the force constants for bond stretching and bond bending, respectively, $r_0$ and $\theta_0$ denote the equilibrium of bond length and bond angle. $V_n$ is the rotational barrier height and $n$ is the periodicity of rotation. $\tau$ is the dihedral angle in the conformation of molecule in the phase, $\phi$.

The non-bonded energy accounts for the van der Waals and electrostatic energies of the pair-wise sum of all possible interacting atoms $i$ and $j$. To consider the van der Waals energy, the attraction occurs at short range and rapidly dies off as the interacting atoms move apart by a few Angstroms, while the repulsion occurs with the distance of interacting atoms become slightly less than the sum of their radius. Using the Lennard-Jones (L-J) 12-6 potential, the attractive energy falls off as $1/r^6$, whereas the repulsive term is proportional to $1/r^{12}$.

$$U_{vdW} = \sum_{i<j}^{atoms} 4\varepsilon \left( \left( \frac{\sigma}{r_{ij}} \right)^{12} - \left( \frac{\sigma}{r_{ij}} \right)^6 \right) \tag{16}$$

where $\varepsilon$ is the well depth of the L-J potential energy, $r$ is the distance between interacting pair-wise atoms and $\sigma$ is the finite particles distance which potential energy is zero.
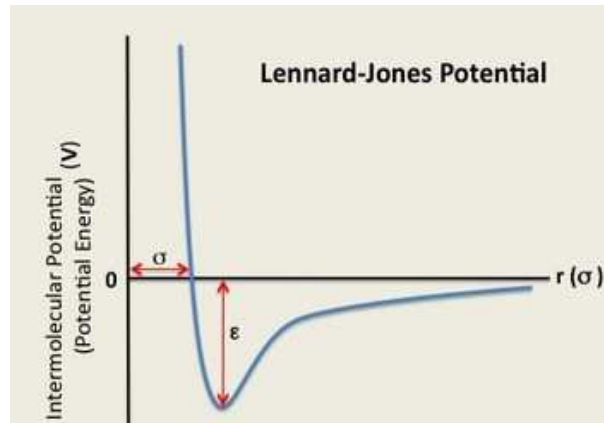
**Figure 2.2** van der Waals energy based on Lennard-Jones potential and its parameters, including the potential well depth ($\varepsilon$), the distance between pair-wise atoms ($r$) and the finite particles distance at zero potential energy ($\sigma$) [UC Davis ChemWiki by University of California, 2012: online].

Consequently, the electrostatic energy relies on the Coulomb's law corresponding to the atomic charges, $q_i$ and $q_j$, of atoms $i$ and $j$, respectively, where D is the effective dielectric constant.

$$U_{ele} = \sum_{i<j}^{atoms} \frac{q_i q_j}{D r_{ij}} \tag{17}$$

Therefore, the potential energy can be written as equation (18).

$$U = \sum_{bonds} k_b (r - r_0)^2 + \sum_{angles} k_\theta (\theta - \theta_0)^2 + \sum_{dihedrals} \frac{V_n}{2} (1 + \cos[n\tau - \phi])$$

$$+ \sum_{i<j}^{atoms} 4\varepsilon \left( \left(\frac{\sigma}{r_{ij}}\right)^{12} - \left(\frac{\sigma}{r_{ij}}\right)^{6} \right) + \sum_{i<j}^{atoms} \frac{q_i q_j}{D r_{ij}} \tag{18}$$

### 2.1.4 Integration algorithm

Once the potential energy was determined, the position and velocity of atoms based on equation of motion can be predicted at time $t + \delta t$ using integration algorithm. There are numerous algorithms such as Verlet algorithm, leapfrog algorithm, Beeman's algorithm etc. All integration algorithms approximate the

positions, velocities and accelerations by Taylor series expansion given in equations (19)-(21).

$$r(t+\delta t) = r(t) + v(t)\delta t + \frac{1}{2}a(t)\delta t^2 + ... \tag{19}$$

$$v(t+\delta t) = v(t) + a(t)\delta t + \frac{1}{2}b(t)\delta t^2 + ... \tag{20}$$

$$a(t+\delta t) = a(t) + b(t)\delta t + ... \tag{21}$$

Integration algorithm which is commonly used for molecular modeling is the Verlet algorithm, writen as following equations.

$$r(t+\delta t) = r(t) + v(t)\delta t + \frac{1}{2}a(t)\delta t^2 \tag{22}$$

$$r(t-\delta t) = r(t) - v(t)\delta t + \frac{1}{2}a(t)\delta t^2 \tag{23}$$

With combinations of these two equations, one gets

$$r(t+\delta t) = 2r(t) - r(t-\delta t) + a(t)\delta t^2 \tag{24}$$

This technique determines the new position at time $t+\delta t$ from the current position and acceleration, as well as the position at time $t-\delta t$, see in equation (24).

### 2.1.5 Steps of MD simulation

The steps of MD simulation are schemed in Fig 2.3. The system needs the energy minimization in order to remove the bad contacts before running MD simulation.

Give initial configuration ($r_0$)

↓

Calculate force ($F$) and acceleration ($a$)
of each atom at the time

↓

Move atom to new position with calculated force for time $t+\Delta t$

↓

Does system reach equilibrium?  —— No

↓ Yes

Collect trajectories and then calculate the properties of system
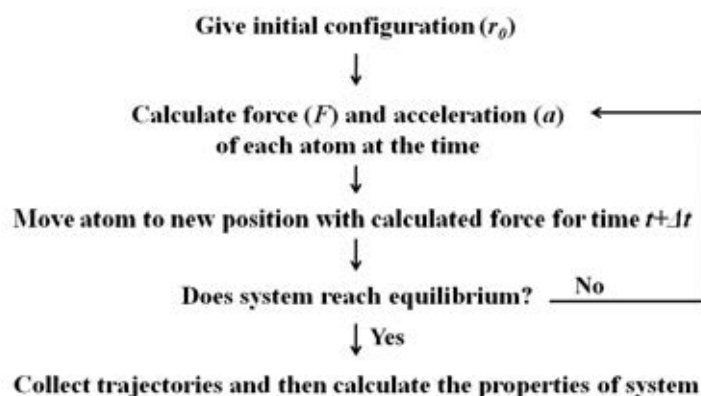
**Figure 2.3** Schematic of MD simulation steps

The MD simulation is performed with following steps.

1.  The initial positions or coordinates ($r_0$) are obtained from the experimental structure by X-ray or NMR spectroscopy. The starting velocity ($v_0$) is generated using random number generator from the Maxwell-Boltzmann or Gaussian distribution.

2.  The force ($F$) and acceleration ($a$) are derived from the potential energy according to Newton's second law of motion.

3.  The atoms are moved to the new positions at the time $t + \delta t$ by the calculated force which is predicted using integral algorithm.

4.  The stability of simulation system is monitored by considering the energy, temperature and global root mean square deviation (RMSD).

5.  After the system reaches the equilibrium, the collection of trajectories is then used for analysis.

**2.1.6 Ensemble**

An ensemble is the collection of replications of the system. All replications share the same properties and specific constraints, but each individual replication is independent. The type of the ensemble is classified by the conditions of a particular thermodynamic state. The different ensembles are described below.

- Microcanonical ensemble (NVE): the total number of atoms (N), volume (V) and energy (E) are constrained to be constant which correspond to an isolated system.

- Canonical ensemble (NVT): the total number of atoms (N), volume (V) and temperature (T) are fixed.

- Isobaric-Isothermal ensemble (NPT): the total number of atoms (N), pressure (P) and temperature (T) are constrained to be constant. Note that this ensemble was chosen in this study.

### 2.1.7 Particle-mesh Ewald

The non-bonded interaction cutoff is applied for the large molecular system in order to save the computing times. The Particle-mesh Ewald (PME) method is basically developed from the Ewald summation which computes the electrostatic energies of periodic system [Darden, York, and Pedersen, 1993]. This method offers the higher efficiency and accuracy, and accomplish for the MD simulation.

### 2.1.8 Water model

In the explicit solvation model, the classical water model is used as the solvent. Many different water models have been proposed with the approximation of molecular mechanics. The three-site (3-site) water models which are the three interaction sites corresponding to the three atoms of water molecule, have been carried out for molecular dynamics simulations. For protein modeling, the transferable intermolecular potential three-position (TIP3P) model is chosen to treat the solvent with the OH distance of 0.9572 Å and the HOH angle of 104.52 degree [Jorgensen et al., 1983].

## 2.2 Solvation structure

The molecular liquid or solvent is the great concern for chemistry. In this work, we aim to understand how solvent affects the protein conformational changes. The theory of liquid can be used to answer this question. Here, two methods, radial

distribution function (RDF) and 3D-RISM approach, were employed to explore the stability of protein in solution.

### 2.2.1 Radial distribution function
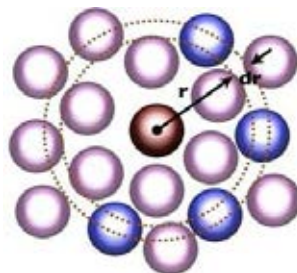


**Figure 2.4** Illustration of radial distribution function, *g(r)*, where the probability of finding the particle (blue atoms) at a radius of *r* away from a reference particle (red atom) [Materials digital library pathway, 2008 : online]

Radial distribution function (RDF) describes the behavior of liquid as the function of distance that has been successful in study of liquid and liquid mixture [Hirschfelder, Stevenson, and Eyring, 1937; Matteoli et al., 1995]. In particular, RDF calculates the probability, $g_{ij}(r)$, of finding the particles *j* (blue) around the selected atom *i* (red) within the sphere of *r* radius as depicted in Figure 2.4. This algorithm involves determining the number of atoms whose centres lie between these two spheres (*dr*) and repeat this process for a number *N* of atoms [Hinchliffe, 2008]. As a results, the $g_{ij}(r)dr$ is expressed in the following equation.

$$g(r)dr = \frac{1}{N}\sum_{i=1}^{N} g_i(r)dr \tag{25}$$

### 2.2.2 3D-RISM calculation

The 3D reference interaction site model (3D-RISM) complemented with the Kovalenko-Hirata (KH) closure relation is a statistical mechanical integral equation [Fumio, 2003] providing the information of the solvation structure both electrostatic and nonpolar features such as hydrogen bond, hydrophobicity, salt bridges, structural solvent [Genheden et al., 2010]. This method has been coupled with ab-initio quantum theory in a self-consistent description of electronic structure for optimizing

the geometry of solution. The general idea of the solvation structure is the probability density of the solvent contribution around the solute molecule in 3D space [Yoshida et., 2008]. This density distribution can be defined as $\rho_\gamma g_\gamma(r)$, a product of average density of the solvent bulk ($\rho_\gamma$) times the 3D distribution function at the $r$ position of solvent molecules around the solute molecule ($g_\gamma(r)$).

The 3D-RISM integral equation was derived from the molecular Ornstein - Zernike (MOZ) equation.

$$g_\gamma(r) = h_\gamma(r) + 1 \tag{26}$$

$g_\gamma(r)$ is the pair correlation function and $h_\gamma(r)$ is the total correlation function of solvent site $\gamma$ in 3D space.

$$h_\gamma(r) = \sum \int dr' c_\alpha(r - r') \chi_{\alpha\gamma}(r') \tag{27}$$

$$c_\gamma(r) \approx \frac{-u_\gamma(r)}{k_B T} \tag{28}$$

$$\chi_{\alpha\gamma}(r) = \omega_{\alpha\gamma}(r) + \rho_\alpha h_{\alpha\gamma}(r) \tag{29}$$

$c_\alpha(r)$ is the direct correlation function where $u_\gamma(r)$ is the 3D interaction potential between the entire of solute and solvent site $\gamma$, and $k_B T$ is the Boltzmann constant.

$\chi_{\alpha\gamma}(r)$ is the site-site susceptibility of the pure solvent, the sum of intramolecular and intermolecular terms.

$$\omega_{\alpha\gamma}(r) = \frac{\delta_{\alpha\gamma}\delta(r) + (1 - \delta_{\alpha\gamma})\delta(r - l_{\alpha\gamma})}{4\pi l_{\alpha\gamma}{}^2} \tag{30}$$

$\omega_{\alpha\gamma}(r)$ is represented as the intramolecular correlation function, while the $h_{\alpha\gamma}(r)$ is the radial total correlation function between $\alpha$ and $\gamma$ site of solvent molecule.

## 2.3 MM/PBSA and MM/GBSA approaches

The molecular mechanic Poisson-Boltzmann surface area (MM/PBSA) and molecular mechanic Generalized Born surface area (MM/GBSA) [Srinivasan, 1998; Kollman et al., 2000; Massova and Kollman, 2000] are the methods for the binding free energy calculation that combines molecular mechanic energy with the implicit solvation model. The basic idea of these methods is the difference in free energies of the three reactants.

$$[receptor]_{aq} + [ligand]_{aq} \rightarrow [complex]_{aq} \tag{31}$$
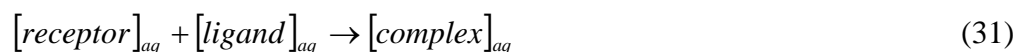
$$\Delta G_{bind} = \Delta G_{complex} - \Delta G_{receptor} - \Delta G_{ligand} \tag{32}$$

The free energy of each reactant contains the enthalpy and entropy contributions.

$$\Delta G = \Delta H - T\Delta S \tag{33}$$

$$\Delta G = \Delta E_{MM} + \Delta G_{solv} - T\Delta S \tag{34}$$

The $\Delta H$ can be represented by the summation of the molecular mechanics gas-phase energy ($E_{MM}$) and the solvation energy ($\Delta G_{solv}$), while the entropy term ($T\Delta S$) is the product of the absolute temperature and the entropy relating to the conformational change in protein. The $E_{MM}$ consists of the internal energy (from bonds, angles and dihedral angles) as well as the non-bonded electrostatic and van-der Waals energies.

$$\Delta E_{MM} = \Delta E_{int} + \Delta E_{ele} + \Delta E_{vdW} \tag{35}$$

The solvation energy ($\Delta G_{solv}$) is the summation of polar ($G_{solv}^{polar}$) and nonpolar ($G_{solv}^{nonp}$) solvation energy.

$$G_{solv} = G_{solv}^{polar} + G_{solv}^{nonp} \tag{36}$$

The nonpolar contribution to the solvation free energy was determined via solvent-accessible surface area, SASA [Sitkoff, Sharp, and Honig, 1994]. The SASA is the surface area of protein accessible to solvent. As Fig. 2.5, the SASA of the red

protein particles was depicted with black dashed line by tracing the center of the probe blue sphere with $r$ radius.
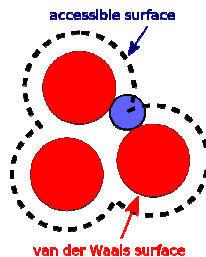


**Figure 2.5** Schematic of solvent-accessible surface area of the red particles (black dash) as well as their van der Waals surface of each atomic radius (red) [Wikipedia, 2012 : online].

The surface area of the protein, which is accessible to solvent, is computed with Paul Beroza's molsurf program [Connolly, 1983].

$$G_{solv}^{nonp} = \gamma SASA \tag{37}$$

where $\gamma$ was achieved from the experimental data of 0.0072 kcal mol$^{-1}$Å$^2$

Both of MM/PBSA and MM/GBSA approaches use the same calculations for molecular mechanic energy ($E_{MM}$) and nonpolar contribution of solvation energy ($G_{solv}^{polar}$), while the electrostatic solvation energy is calculated using Poisson-Boltzmann (PB) equation [Fogolari, Brigo, and Molinari, 2002] or generalized Born (GB) model [Still, 1990; Jayaram, Sprous, and Beveridge, 1998]. The electrostatic potential ($\phi$) of MM/PBSA approach is computed by solving the PB equation implemented in the pbsa program [Gilson and Honig, 1988].

$$\nabla \varepsilon(r) \nabla \varphi(r) = -4\pi \rho(r) - 4\pi \sum_i z_i c_i \exp(\frac{-z_i \phi(r)}{k_B T}) \tag{38}$$

$\varepsilon(r)$ is the dielectric constant. $\phi(r)$ is the electrostatic potential. $\rho(r)$ is the solute charge and $z_i$ is the charge of ion type $i$. $c_i$ is the number density of ion type $i$ far from the solute. $k_B$ is the Boltzmann constant and T is the temperature. Finally, the summation is over all different ion types.

In this work, the binding affinities of oseltamivir toward NAs, including wild-type, E119G, R152K and D198N, were determined using MM/PBSA method implemented in the AMBER program. Although the substitutions on NA gene associate with the conformational changes of the oseltamivir binding pocket but the results in entropy contribution of all systems are assembly similar. Thus, this entropy term is neglected from the binding free energy calculation.

## 2.4 Per-residue decomposition energy

The contribution of individual residue or called per-residue decomposition energy can use to identify the key residues for inhibitor binding. Since amino acid composes of backbone and side chain parts, the decomposition energy not only present as the per-residue total binding free energy but also as backbone and its side chain contribution. To consider the interaction between drug and each binding residues of protein, the atoms belonging to the drug was assigned as $i$, while $j$ is the atoms of the protein. The electrostatic energy ($E_{ele}^i$) is of one half of a pairwise charge-charge interaction between $i$ and $j$ atoms, as expressed in (39). Likewise, the one half of the pairwise drug-target van der Waals interaction ($E_{vdW}^i$) is also measured.

$$E_{ele}^i = \frac{1}{2}\sum_j \frac{q_i q_j}{r_{ij}} \tag{39}$$

The decomposition of the free energy on a per-residue basis was estimated using MM/GBSA approach. As previously stated, this approach uses the GB model, as given by (x), instead the PB equation to solve the polar solvation energy.

$$G_{solv}^{pol} = -\frac{1}{2}\left(1 - \frac{e^{-\kappa f_{GB}}}{\varepsilon_\omega}\right)\sum_{ij} \frac{q_i q_j}{f_{GB}} \tag{40}$$

where $\varepsilon_\omega$ is the dielectric constant of solvent, $\kappa$ is the Debye-Hückel parameter and the double sum run over all pairs of atoms. In this work, the $\varepsilon_\omega$ and $\kappa$ were allocated

as 80 and 1, respectively. The $f_{GB}$ is a certain smooth function of its argument as given below.

$$f_{GB} = \left[ r_{ij}^2 + \alpha_i \alpha_j \exp\left( \frac{-r_{ij}^2}{4\alpha_i \alpha_j} \right) \right]^{1/2} \tag{41}$$

where $r_{ij}$ is the distance between atoms $i$ and $j$, the $\alpha_i$ and $\alpha_j$ are so called the effective Born radius of atoms $i$ and $j$, respectively. In addition, the calculation of per-residue decomposition energy was performed using the LCPO method for SASA calculation [Weiser, Shenkin, and Still, 1999] and the Onufriev GB model developed by Onufriev and coworker [Onufriev et al., 2004].

# CHAPTER III

# METHODOLOGY

## 3.1 Preparation of systems

All preparing systems of MD simulation were done using the AMBER 10 software package [Case et al., 2008]. The crystal structure of B/Beijing/1/87 wild-type NA in complex with sialic acid, Protein Data Bank (PDB) code 1NSC [Burmeister et al., 1993], was chosen to use as the starting structure for all oseltamivir-NA complexes. To construct the wild-type and oseltamivir complex, this sialic acid was replaced by the oseltamivir structure taken from the PDB code 2HU4 [Russell et al., 2006], while the crystallographic calcium ions and water molecules were conserved. Then, this system was used as the template for preparing the three variants, E119G, R152K and D198N by single residue mutation to the residue of interest (residue position in Fig. 3.1) using the Leap module in AMBER. The ionizable residues (K, R, D, E and H) were considered their protonation state at pH 7.0. All missing hydrogen atoms of the protein and ligand were added using the LEaP module and were then minimized in order to remove the bad contacts. Each system was neutralized by the counter ions and immersed in a TIP3P [Jorgensen et al., 1983] water box that extended at least 13 Å from the protein surface. The AMBER03 force field was employed for all protein atoms [Duan et al., 2003], while the force field and RESP charge of oseltamivir were retrieved from our previous work [Malaisree et al., 2008].
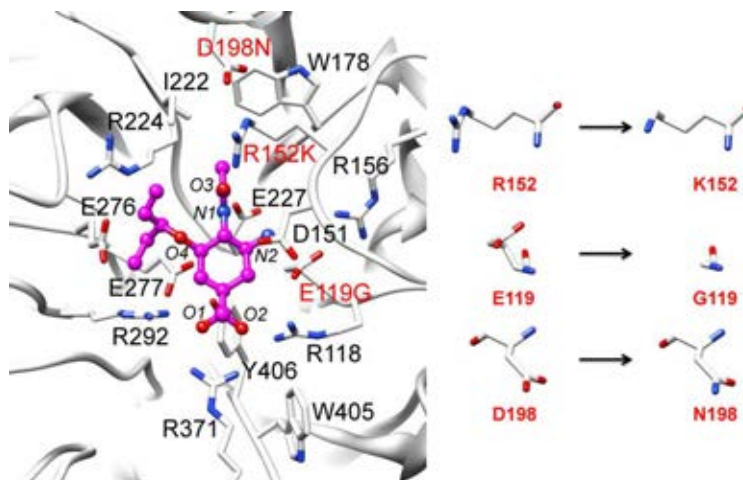
**Figure 3.1** Oseltamivir (bond and stick model) and its binding residues of influenza B NA wild-type (black) where the three residues (red) are singly mutated for study on the source of oseltamivir resistance: there are E119G, R152K and D198N mutations. The drug heteroatoms are labeled for latter discussion.

## 3.2 Protocol of MD simulation

All calculations were performed using the SANDER module implemented in AMBER. Only the solvent molecules were first optimized and consequently the whole system was minimized with 1,000 steps of steepest descent and 2,000 steps of conjugate gradient. For the thermalization step, the temperature of heat bath applied for each system was gradually increased from 10 to 310 K with 2.0 fs of time step for 100 ps. After target temperature was reached, the simulated system was maintained at this temperature for 100 ps using weak-coupling algorithm [Berendsen et al., 1984]. All atomistic MD simulation was run at 310 K and 1 atm using the periodic boundary condition and the NPT ensemble. The SHAKE algorithm was applied to constrain the bond length involved the hydrogen atoms [Ryckaert, Ciccotti, and Berendsen, 1977] and Particle mesh Ewald (PME) was used to treat the long-range electrostatic interaction [Darden et al., 1993]. The nonbonded interaction cutoff was 12 Å and the time step was 2 fs. Oseltamivir structure and it surrounding residues within 6 Å sphere (R118, E119, D151, R152, R156, D198, I222, E227, E277, R292, N294, R371 and Y406) were positionally restrained with the decreasing force constants of 20, 10,

5, 2.5 kJ/mol/Å$^2$ for 100, 100, 400 and 400 ps, respectively. Then, the unrestraint simulation was performed for 4 ns. To obtain the precision of the drug-target interaction calculation, the three different MD simulations with distinguish starting velocities were treated for each system.

The energy, temperature and global root mean square deviation (RMSD) relative to the starting structure was monitored to verify the stability of simulated system. The production phase of each system was then analyzed in terms of the drug-target interactions, the solvation structures and the oseltamivir binding affinity for understanding the oseltamivir efficiency, the loss of drug-target interaction and binding free energy in the three single mutants.

## 3.3 3D-RISM calculation

The 3D-RISM approach was employed on both wild-type and three mutant strains to explore the solvation structure. The last 5-ns snapshot of MD simulation was used for the calculation, where the water molecules and the treated ions were striped. The KH approximation was applied for closing the 3D-RISM equation with the advantage of rapid convergence [Kovalenko and Hirata, 1999: 2000]. The potential parameter and structure of TIP3P water molecules were adopted from previous work [Phongphanphanee, Yoshida, and Hirata, 2008; Phongphanphanee et al., 2010]. The structure was centered in the box size $90 \times 90 \times 90 \, \text{Å}^3$ with the grid spacing of $180 \times 180 \times 180 \, \text{points}$. The AMBER force field was adopted to solve the potential energy of the protein.

# CHAPTER IV

# RESULTS AND DISCUSSION

## 4.1 The stability of system

The stability of all systems was accessed by considering the plot of root mean square displacement (RMSD) of MD structures versus simulation time in respect with the initial structure, shown in Fig. 4.1. The RMSD for protein backbone atoms of the three different simulations of each system was separately plotted. All systems were found to reach an equilibrium state at 3 ns, and thus the trajectories extracted from the last 2 ns of all three simulations were further analyzed.
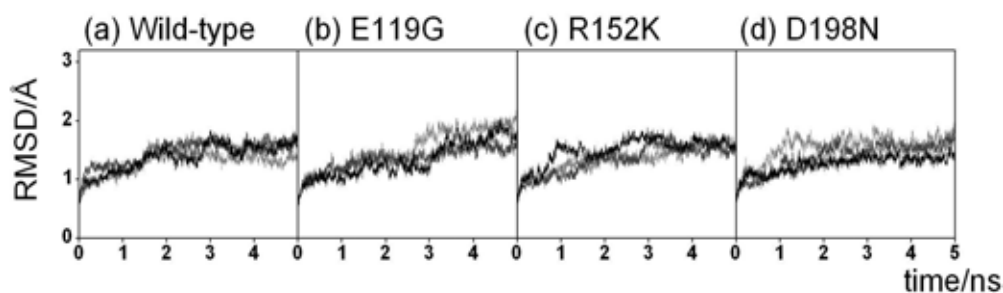


**Figure 4.1** The plot of RMSD for protein backbone atoms versus simulation time of (a) Wild-type, (b) E119G, (C) R152K and (d) D198N with the three different starting velocities (black, dark grey and light grey).

## 4.2 Drug-target binding interactions

To seek the drug-target interactions of influenza B NA on both wild-type and three mutant systems, the individual residue energy contributed to oseltamivir and hydrogen bond formation were evaluated using the MM/GBSA and ptraj modules, respectively, in AMBER.

### 4.2.1 Per-residue decomposition energy

The decomposition free energy based on the per-residue ($\Delta G_{bind}^{residue}$) using MM/GBSA approach [Gohlke, Kiel, and Case, 2003; Zoete, Meuwly, and Karplus, 2005; Rungrotmongkol et al., 2010] was carried out to identify the key residues involved in oseltaimivir binding to the active site of influenza B NA. The results are summarized in Fig. 4.2.
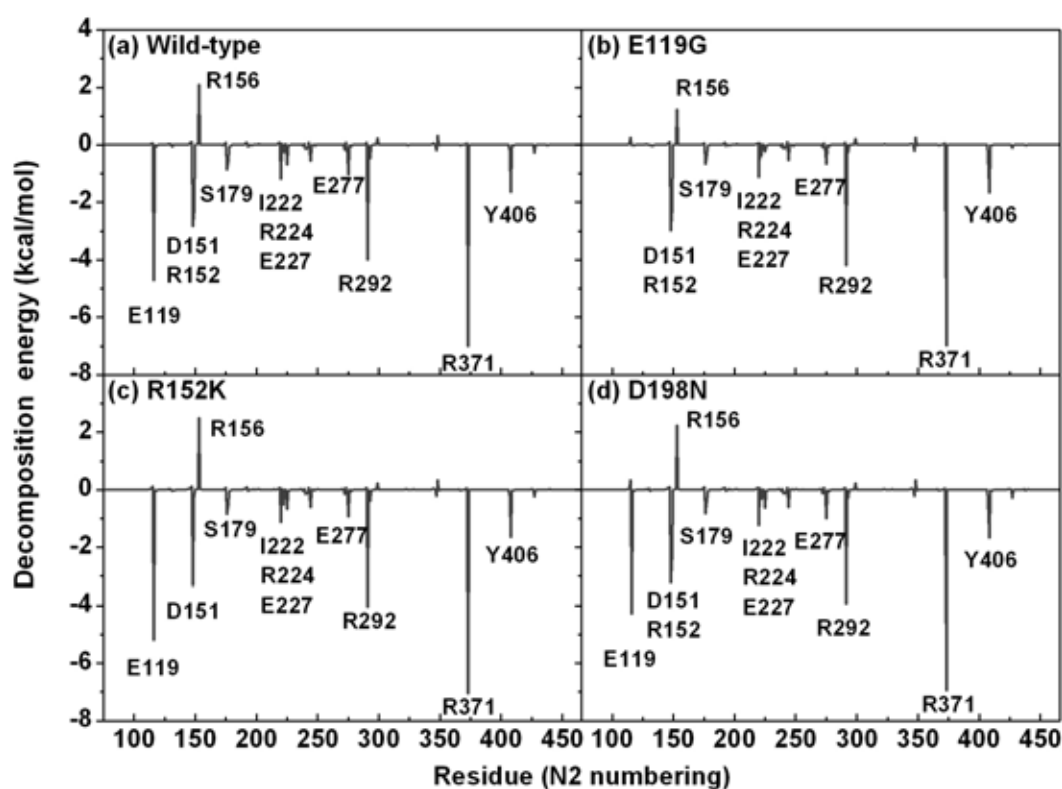


**Figure 4.2** Decomposition energy on the basis of per-residue for all NA residues averaged over the three different simulations of (a) wild-type, (b) E119G, (c) R152K and (d) D198N.

The residue with negative energy value means the stabilization of oseltamivir binding and in *vice versa*. The fingerprint of per-residue decomposition energy in all systems shows that only residues in the active and framework sites of NA play the responsibility for oseltamivir binding. Although they likely show the stabilized

contribution toward oseltamivir, the repulsive interaction between the guanidinium group of R156 and the ammonium group of drug provides the energy destabilization of c.a. 2 kcal/mol in all systems except for E119G mutant (1 kcal/mol). Hence, the $\Delta G_{bind}^{residue}$ as well as their backbone ($\Delta G_{bind}^{backbone}$) and side chain ($\Delta G_{bind}^{sidechain}$) of the residues in the catalytic site (R118, D151, R/K152, R224, E276, R292, R371 and Y406), framework site (E/G119, R156, W178, S179, D/N198, I222, E227, H274, E277, N294 and E425) and two distinct residues nearby framework (G347 and W405) are focused and given in Fig. 4.3 (left). In addition, the residue energy contribution in terms of electrostatic ($E_{ele}+G_{polar}$) and van der Waals ($E_{vdW}+G_{nonpolar}$) was also shown in the same figure (right).

In Fig. 4.3 (left), it can be seen that the side chain atoms of all 21 residues provided the major contribution to the binding free energy per-residue basis, $\Delta G_{bind}^{residue}$, for the binding of oseltamivir in the NA active site. Among these residues of wild-type, oseltamivir was highly stabilized by the five catalytic residues D151, R152, R292, R371 and Y406, and the framework residue E119 with $\Delta G_{bind}^{residue}$ in range of -1.6 to -7.0 kcal/mol. Most of them (except for R152 and Y406) give the individual contribution in term of electrostatic energy (Fig. 4.3a, right) rather than vdW energy. Besides the electrostatic term, the residues with favorable vdW energy are valid for the hydrophobic contact in protein-ligand association. The R152, R224 and E276 in the catalytic sites and W178, I222, E277 and Y406 in framework sites likely presented the vdW energy contribution (-0.9 to -2.0 kcal/mol) toward oseltamivir. The salt bridge formation between R224 and E276 established the well-known hydrophobic pocket to occupy the bulky group ($-OCHEt_2$) of oseltamivir, whereas the hydrophobic pocket formed by R152, W178, I222 and R224 accommodated the methyl group of the –NHAc moiety of oseltamivir [Taylor and Russell, 2009].
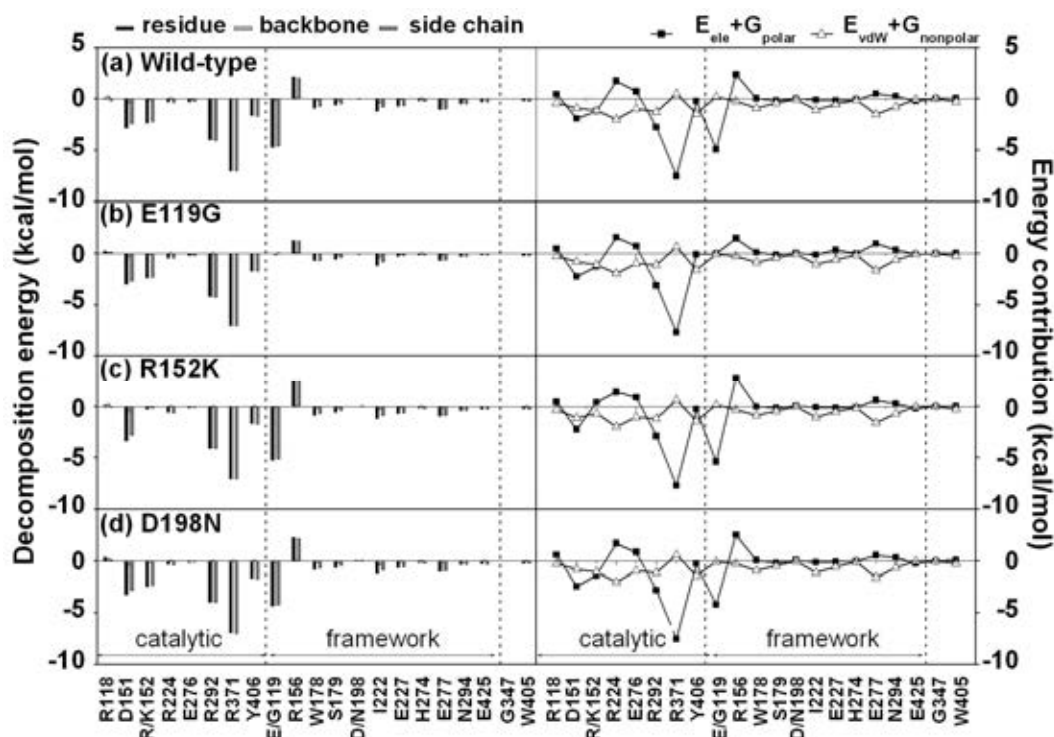
**Figure 4.3** (Left) The binding free energy in pairwise per-residue basis ($\Delta G_{bind}^{residue}$), and its energy contributions from the backbone ($\Delta G_{bind}^{backbone}$) and side chain ($\Delta G_{bind}^{sidechain}$) atoms for the residues in the catalytic and framework sites as well as the two additional residues nearby framework site for the four complexes studied, where their electrostatic ($E_{ele}+G_{polar}$) and van der Waals ($E_{vdW}+G_{nonpolar}$) energy terms were presented in the right-hand side.

In comparison to the wild type, the entire loss of oseltamivir contribution were found at the mutated residues, G119 in E119G mutant and K152 in R152K mutant (Fig. 4.3b-c, left), while the mostly conserved contribution was observed in the D198N system (Fig. 4.3d, left). For the first two mutations, the mutated residues G119 and K152 only decreased the electrostatic energy contribution by 4.9 and 1.6 kcal/mol, respectively, whereas the vdW energy contribution was relatively similar to that of wild-type (Fig. 4.3b-c, right). The noticeable reduction in electrostatic contribution of the E119G mutant was associated with the substitution of nonpolar and short residue G119 instead of the negatively charged polar residue of the E119. In contrast for R152K mutant, the alteration from the positive charge with long chain of

arginine became the same total charge but shorter side chain of lysine has affected a smaller decrease in the electrostatic interaction.

### 4.2.2 Hydrogen bond

By following the per-residue decomposition energy calculation, the key binding residues E119, D151, R152, R292 and R371 provided the dominant electrostatic stabilization in oseltamivir binding at the NA active site. Since the hydrogen bond interaction is an important factor in electrostatic attraction, the hydrogen bond formation between the oseltamivir and the NA residues were determined on the basis of a maximum distance of 3.5 Å between hydrogen donor (D) and acceptor (A), and a minimum bond angle of 120 degree for D_H…A. The results of the averaged hydrogen bonds over the three different MD simulations for both wild-type and mutants are plotted and compared in Fig. 4.4, where their representative structures taken from the last trajectory of the first-run simulation were depicted on the right-hand side.
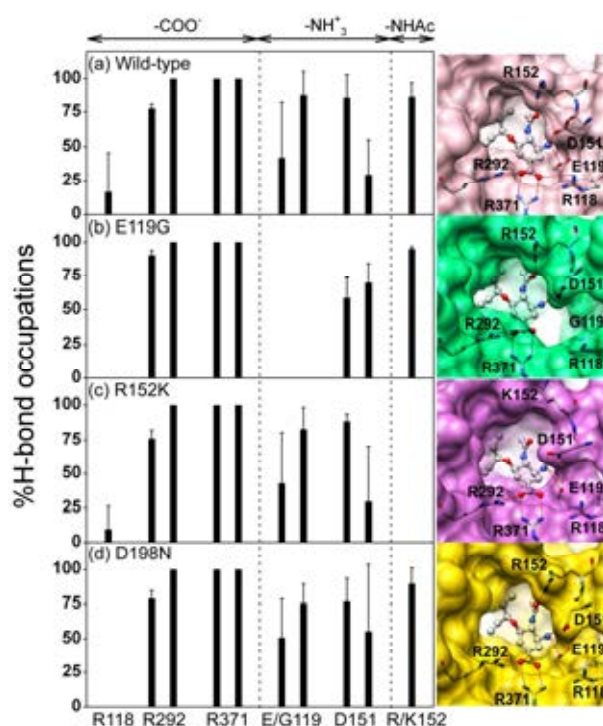
**Figure 4.4** (Left) Percentage occupation of hydrogen bonds averaged over three-time simulations for the four systems studies: (a) wild-type, (b) E119G, (c) R152K and (d) D198N, where the standard deviation values are also given. (Right) Close up of oseltamivir (bond and stick model) in the NA binding pocket (surface) from the representative structure of each system and its hydrogen bond formation with the surrounding residues are shown by red dashed line.

As expected, the residues E119, D151, R152, R292 and R371 in wild-type system form the strong hydrogen bonds (>75%) with the three functional groups of oseltamivir as seen in Fig. 4.3a. Although the –COO⁻ group was strongly interacted with the two conserved arginines R292 and R371, the other one, R118, formed hydrogen bond with this group only 17%. This is a consequence of the rotation of the Y406 phenol ring which repelled R118 away from oseltamivir (Fig. 4.5). The observation was somewhat similar to what found in the oseltamivir-NA complex of influenza A/H5N1 virus [Malaisree et al., 2008, Udommaneethanakit et al., 2009] but loss of R118 interaction was compensated with the moderate hydrogen bond with the residue Y347 located nearby framework site. It is a worth to note that this is in contrast to the case of influenza B NA (Table 1.2) whereas G347 cannot stabilize the

–COO⁻ group, perhaps explaining a lower susceptibility of oseltamivir toward the influenza B virus than the influenza A virus [Gubareva et al., 2000; Kawai et al., 2005; Mishin et al., 2005; Sugaya et al., 2007]. In addition, the results of three distinguish 5-ns simulations demonstrated that the 150-loop was always in the closed conformation while the high flexibility was observed in the 430-loop in both wild-type (Fig. 4.5) and mutants (data not shown). The open conformation of the 150-loop in influenza B NA might be possible as found in the long MD simulations of H5N1, pH1N1 and H2N2 NAs [Amaro et al., 2011].
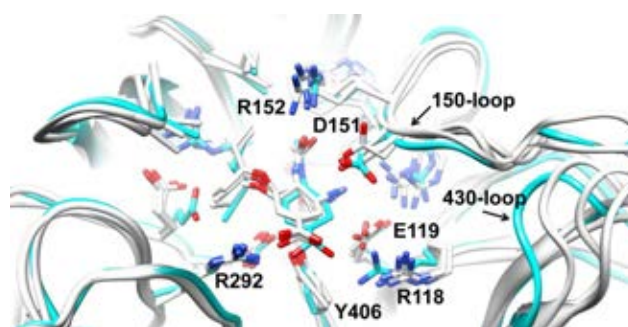


**Figure 4.5** Superimposition of the last snapshot from the three different simulations (grey) of the wild-type on the initial structure (cyan) demonstrates the rotation of Y406 phenol ring in MD snapshots repelled residue R118 away from oseltamivir.

To reveal the effect of substitution on NA gene to the oseltamivir binding into the active site, the hydrogen bond results of the three single mutants E119G, R152K and D198N were compared in respect to those of wild-type. Note that only the significant change of hydrogen bond occupation due to mutation was extensively discussed. At the –COO⁻ moiety, the R292 and R371 were likely conserved for all mutant systems (Fig. 4.4b-d), whereas the R118 totally lost the interaction for the E119G and D198N variants, and the slightly reduced interaction (to 10%) was detected in the R152K system. Important difference at the $–NH_3^+$ site was noticed in the E119G system (Fig. 4.4b) in which the mutated G119 had no hydrogen bond contribution to the $–NH_3^+$ group as same as what found in the previous studies on drug binding to influenza A/pH1N1 E119V [Rungrotmongkol et al., 2010] and E119A [Pan et al., 2011] strains. This finding is supported by the no electrostatic

energy contribution by G119 ($\Delta G_{bind}^{residue}$ = 0 kcal/mol in Fig. 4.3b, right). For the –NHAc group, the disappearance of interaction was only found at the mutated residue K152 in the R152K mutant (Fig. 4.4c) like the MD result of zanamivir-R152K system in pH1N1 virus [Pan et al., 2011]. In the present study, the side chain of K152 flipped to form the salt bridge interaction with D198 (Fig. 4.4c, right), and resulted in decrease of electrostatic energy to positive value (in Fig. 4.3c, right). Although almost all interactions were considerably conserved in the D198N mutant, slight decrease in hydrogen bond occupation was presented at the E119 and D151 and again no interaction formed with R118.

## 4.3 Ligand solvation

The solvent, especially water, is essential for the stability and function of protein. Change in protein conformation due to the substitution of amino acid can affect the cluster of water molecules in the binding pocket. The accessibility of water molecules between the oseltamivir molecule and the NA pocket can reduce the strength of oseltamivir binding. To analyze this effect, the radial distribution function (RDF) based on all MD trajectories in production phase was employed to determine the surrounding waters around the oseltamivir molecule in the complex. The RDF, $g_{ij}(r)$, is the probability of finding the particles $j$ around the selected atom $i$ within the sphere of $r$ radius. Here, $i$ represents all heteroatoms of oseltamivir O1, O2, O3, O4, N1 and N2 (see the labeled atoms in Fig. 3.1) while $j$ is the water oxygen atom. The RDF results with the coordination number, $n(r)$, of the surrounding solvent molecules are schemed in Fig. 4.6.
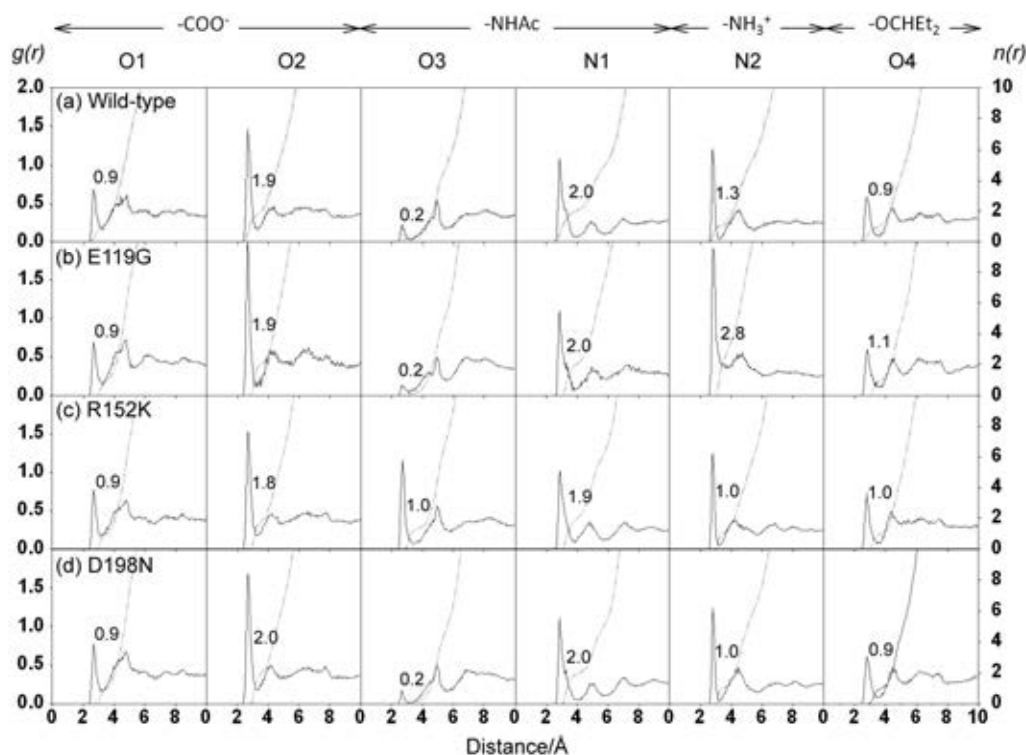
**Figure 4.6** Radial distribution function, *g(r)*, between all heteroatoms of oseltamivir (atomic labels shown in Fig. 3.1) and O-water atoms was illustrated in the left axis, while the coordination number, *n(r)*, of each system was integrated up on the right axis. The accessible water numbers integrated up to the first minimum are also given.

From the RDF calculation (Fig. 4.6a), all graphs of oseltamivir heteroatoms (except for the O3 atom) in wild-type showed the first sharp peak at approximately 3 Å suggesting that the accessible water molecules strongly interact with the interested atoms. The O1 and O2 atoms of –COO⁻ group were solvated by the one (w1) and two (w2 and w3) water molecules, respectively (waters in bond and stick model, Fig. 4.7a). The O3 atom of –NHAc moiety directly interacts to the R152, thus, no water can be occupied. In contrast, the N1 atom of this side chain was strongly solvated by two bridging water molecules (w4 and w5 in Fig. 4.7a), as seen by the value at the first minimum nearly closed to zero, to keep the oseltamivir-NA interaction through hydrogen bond network with the framework residues W178, E227 and E277. The

surrounding w4-water also bridged with the N2 atom of $-NH_3^+$ group, whereas the O4 atom of bulky group was solvated by a water molecules (w6).
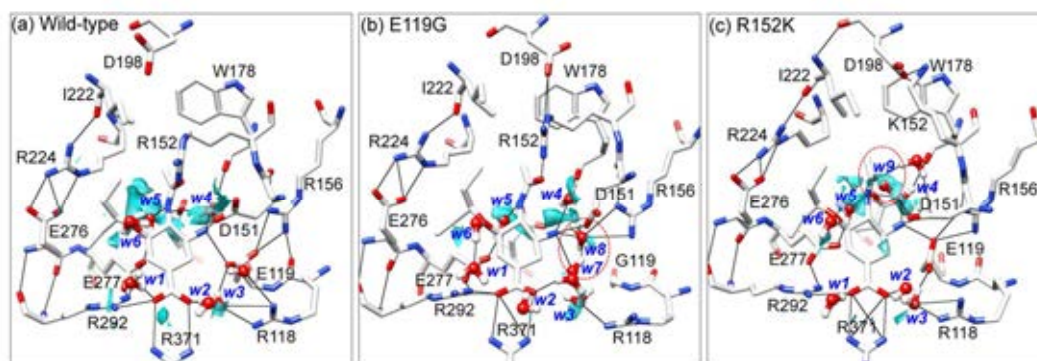


**Figure 4.7** 3D-distribution function of O-water atoms with *g(r) > 4* using the 3D-RISM approach (cyan surface), and the water molecules (ball and stick model) from the last MD snapshot of wild-type and two single mutants, E119G and R152K, where the hydrogen bond network involving waters are illustrated by black line.

Among the three mutant systems, the RDF results of D198N (Fig. 4.6d) were very similar to those of the wild-type while noticeable difference was found in the E119G and R152K mutants at the oseltamivir's side chain directly interacted with the residue substitution (Fig. 4.6b-c). Therefore, the latter two mutated systems were further analyzed and extensively discussed in relative to wild-type in terms of the RDF and the advanced 3D-RISM results. The 3D-RISM has shown a success theory for exploring the solvation structure around the solute molecules which are oseltamivir and NA protein in three-dimension (3D). The 3D-distribution of the water oxygen atom with the distribution function greater than 4, *g(r) > 4*, within 2.5 Å sphere of oseltamivir was depicted in Fig. 4.7. The water contribution based on 3D-RISM was painted in cyan, while the existed water structures from the last MD snapshot (the ball and stick model) were also presented for comparison.

The 3D distribution function of water with *g(r) > 4* for wild-type system in Fig. 4.7a clearly showed the water contribution around the O2, N1 and N2 atoms of

oseltamivir in correspondence to the sharp and high probability of RDFs in Fig. 4.6a. By considering the E119G system, the larger cavity due to the substitution of the short and nonpolar residue G119 (Fig. 4.4b, right) has induced two more water accessibility, w7 and w8 in Fig. 4.7b, (increased from one water molecule w4 in wild-type) at the $-NH_3^+$ group. Since these two added waters were in turn their positions quite frequently as indicated by the first minimum value of 2 in Fig. 4.6b, their 3D-distribution function were relatively smaller than the w4 molecule (Fig. 4.7b). Moreover, the three waters in this area established hydrogen bond network linking between the $-NH_3^+$ group of oseltamivir and the NA residues R156, W178. Likewise, the O3 atom of oseltamivir's –NHAc group in R152K mutant (Fig. 4.6c) was almost strongly solvated by an additional water molecule (w9 in Fig. 4.7c) which was clearly seen by a large O-water contribution located nearby this atom. This is because the larger cavity due to the shorter side chain of K152 flipped out from the active site and formed the salt bridge interaction with D198 as mentioned above.

## 4.4 Oseltamivir binding affinity

The strength of ligand binding affinity can be measured in term of the binding free energy, $\Delta G_{binding}$. Here, the predictions of oseltamivir efficiency against the wild-type and the three mutants over the three different simulations were carried out using Molecular Mechanics/Poisson-Boltzmann Surface Area (MM/PBSA) approach. Generally, the well-known MM/PBSA for the ligand affinity estimation was described in previous studies [Kollman et al., 2000; Aruksakunwong et al., 2007, Malaisree et al.,2009]. The predicted $\Delta G_{binding}$, its components and the experimental $\Delta G_{binding}^{IC_{50}}$ converted from $IC_{50}$ values [Jackson et al., 2005; Mishin et al., 2005] were summarized in the Table 4.1. Besides, the relative energy, the difference of binding free energy between mutant and wild-type system, was determined to evaluate the accuracy of MM/PBSA approach also shown in Table 4.1.

**Table 4.1** The MM/PBSA binding free energies ($\Delta G_{binding}$) of oseltamivir towards of the wild-type and mutant NA strains of the influenza B virus in comparison to the experimental $\Delta G_{binding}$ converted from the $IC_{50}$ values [Jackson et al., 2005; Mishin et al., 2005]. The averaged value and standard deviation of the predicted $\Delta G_{binding}$ are derived from the three different simulations.

| NA strain | | Wild-type | E119G | R152K | D198N |
|---|---|---|---|---|---|
| *Predictive* | | | | | |
| B/Beijing/1987 | $\Delta G_{binding}$ | $-31.4 \pm 2.0$ | $-29.8 \pm 1.4$ | $-26.3 \pm 1.6$ | $-30.3 \pm 2.1$ |
| | **Relative energy** | | **1.6** | **5.1** | **1.1** |
| *Experimental* | | | | | |
| B/Beijing/1987 [Jackson et al., 2005] | $\Delta G_{binding}^{IC_{50}}$ | $-11.9$ | $-9.9$ | $-8.6$ | - |
| | **Relative energy** | | **2.0** | **3.3** | **-** |
| B/Memphis/1996 [Mishin et al., 2005] | $\Delta G_{binding}^{IC_{50}}$ | $-11.4$ | - | $-8.7$ | - |
| | **Relative energy** | | **-** | **2.7** | **-** |
| B/Rochester/2001 [Mishin et al., 2005] | $\Delta G_{binding}^{IC_{50}}$ | $-10.2$ | - | - | $-8.9$ |
| | **Relative energy** | | **-** | **-** | **1.3** |

In Table 4.1, the oseltamivir in complex with wild-type NA showed the lowest binding free energies ($\Delta G_{binding}$) of -31.4 kcal/mol, while the three single mutations have caused the increased free energies of -29.8, -26.3 and -30.3 kcal/mol for the E119G, R152K and D198N mutants, respectively. The reduction in oseltamivir efficiency was as expected from the above results of drug-target interaction and ligand solvation. The single mutations on the key residues 119 and 152, which gave the major contribution to oseltamivir binding, can cause the high level of oseltamivir resistance with the 31- and 252-fold for E119G and R152K mutants of the recombinant B/Beijing/1987 ($\Delta G_{binding}^{IC_{50}}$ in kcal/mol for wild-type: -11.9, E119G: -9.9 and R152K: -8.6) or the 100-fold for R152K mutant of the B/Memphis/1996 isolate (-8.7 kcal/mol increased from -11.4 kcal/mol in wild-type). The completely loss of oseltamivir-NA interaction and the appearance of a water molecule at the –NHAc group were found to be a primary source of high-level resistance due to R152K mutation. Differentially for the E119G mutant, although no interaction was found with the mutated residue G119, the interaction at the –NH$_3^+$ side chain was

maintained via the residue D151 and further stabilized by the hydrogen network with the three waters w4, w7 and w8 which were linked to the framework residues R156 and W178. On the other hand, the mutation on the residue 198 in framework site, that has no direct interaction with oseltamivir, showed likely conserved interactions in comparison to the wild-type. This leads to only the 9-fold resistance to oseltamivir ( $\Delta G_{binding}^{IC_{50}}$ changed from -10.2 kcal/mol in wild-type to -8.9 kcal/mol in D198N).

# CHAPTER V
# CONCLUSIONS


In this research, three different MD simulations were performed on the four modeled complexes of wild-type, E119G, R152K and D198N strains of influenza B NA with oseltamivir bound in order to understand how oseltamivir inhibit influenza B NA and to investigate the source of oseltamivir resistance due to the substitutions on NA gene which were only found in influenza B. From the fingerprint of decomposition energy per-residue basis over 390 residues in wild-type, the five key residues in the binding site (E119, D151, R152, R292 and R371) mainly stabilized the oseltamivir through the strong hydrogen bond formation. The completely loss of oseltamivir-NA interaction and the appearance of a water molecule at the –NHAc group were found to be a primary source of high-level oseltamivir resistance due to R152K mutation. For the E119G mutant, no interaction was found with the mutated residue G119, however, the interaction at the $-NH_3^+$ side chain was maintained via the residue D151 and further stabilized by the hydrogen network with the three waters w4, w7 and w8 which were linked to the framework residues R156 and W178. On the other hand, the mutation on the framework residue 198, which has no direct interaction with oseltamivir, showed likely conserved interactions in comparison to the wild-type. Altogether, the simulated results could explain why and how the single mutations on the key residues 119 and 152 have caused the high-level of oseltamivir resistance with the 31- and 252-fold for E119G and R152K mutants of the B/Beijing/1987 plasmid-based, or the 100-fold for R152K mutant of the B/Memphis/1920 isolate, while the D198N of the B/Rochester/2001 isolate has conferred only 9-fold resistance to oseltamivir. Based on the MM/PBSA binding free energy, the inhibitory potency of oseltamivir against influenza B can be ordered as wild-type> D198N > E119G > R152K, which are in good agreement with the experimental data [Jackson et al., 2005; Mishin et al., 2005].

# REFERENCES

Abed Y., Nehmé B., Baz M. and Boivin G. 2008. Activity of the neuraminidase inhibitor A-315675 against oseltamivir-resistant influenza neuraminidases of N1 and N2 subtypes. Antiviral Research 77: 163-166.

Aruksakunwong O., Malaisree M., Decha P., Sompornpisut P., Parasuk V., Pianwanit S. and Hannongbua S. 2007. On the Lower Susceptibility of Oseltamivir to Influenza Neuraminidase Subtype N1 than Those in N2 and N9. Biophysical Journal 92: 798-807.

Barnett J.M., Cadman A., Burrell F.M., Madar S.H., Lewis A.P., Tisdale M. and Bethell R. 1999. In vitro selection and characterisation of influenza B/Beijing/1/87 isolates with altered susceptibility to zanamivir. Virology 265: 286-295.

Barr I.G., McCauley J., Cox N., Daniels R., Engelhardt O.G., Fukuda K., Grohmann G., Hay A., Kelso A., Klimov A., Odagiri T., Smith D., Russell C., Tashiro M., Webby R., Wood J., Ye Z. and Zhang W. 2010. Epidemiological, antigenic and genetic characteristics of seasonal influenza A(H1N1), A(H3N2) and B influenza viruses: Basis for the WHO recommendation on the composition of influenza vaccines for use in the 2009–2010 Northern Hemisphere season. Vaccine 28: 1156-1167.

Berendsen H.J.C., Postma J.P.M., van Gunsteren W.F., DiNola A. and Haak J.R. 1984. Molecular dynamics with coupling to an external bath. The Journal of Chemical Physics 81: 3684-3690.

Burmeister W.P., Henrissat B., Bosso C., Cusack S. and Ruigrok R.W.H. 1993. Influenza B virus neuraminidase can synthesize its own inhibitor. Structure 1: 19-26.

Case D.A., Darden T.A., Cheatham T.E.I., Simmerling C.L., Wang J., Duke R.E., Luo R., Crowley W., Walker R.C., Zhang W., Merz K.M., Wang B., Hayik S.,

Roitberg A., Seabra G., Kolossváry I.; Wong K.F., Paesani F., Vanicek J., Wu X., Brozell S.R., Steinbrecher T., Gohlke H., Yang L., Tan C., Mongan J., Hornak V., Cui G., Mathews D.H., Seein M.G., Sagui C., Babin V. and Kollman P.A. 2008. AMBER10. San Francisco: University of California,

Collins P.J., Haire L.F., Lin Y.P., Liu J., Russell R.J., Walker P.A., Skehel J.J., Martin S.R., Hay A.J. and Gamblin S.J. 2008. Crystal structures of oseltamivir-resistant influenza virus neuraminidase mutants. Nature 453: 1258-1261.

Darden T., York D. and Pedersen L. 1993. Particle mesh Ewald: An N [center-dot] log(N) method for Ewald sums in large systems. The Journal of Chemical Physics 98: 10089-10092.

Duan Y., Wu C., Chowdhury S., Lee M.C., Xiong G., Zhang W., Yang R., Cieplak P., Luo R., Lee T., Caldwell J., Wang J. and Kollman P. 2003. A point-charge force field for molecular mechanics simulations of proteins based on condensed-phase quantum mechanical calculations. Journal of Computational Chemistry 24: 1999-2012.

Francis T.Jr. 1940. A new type of virus from epidemic influenza. Science 92 : 405-408.

Genheden S., Luchko T., Gusarov S., Kovalenko A. and Ryde U. 2010. An MM/3D-RISM Approach for Ligand Binding Affinities. The Journal of Physical Chemistry B 114: 8505-8516.

Gilson M.K. and Honig B. 1988. Calculation of the total electrostatic energy of a macromolecular system: Solvation energies, binding energies, and conformational analysis. Proteins: Structure, Function, and Bioinformatics 4: 7-18.

Gohlke H., Kiel C. and Case D.A. 2003. Insights into protein–protein binding by binding free energy calculation and free energy decomposition for the Ras–Raf and Ras–RalGDS complexes. Journal of Molecular Biology 330: 891-913.

Gubareva L.V., Matrosovich M.N., Brenner M.K., Bethell R.C. and Webster R.G. 1998. Evidence for zanamivir resistance in an immunocompromised child infected with influenza B virus. Journal of Infectious Diseases 178: 1257-1262.

Gubareva L.V., Kaiser L. and Hayden F.G. 2000. Influenza virus neuraminidase inhibitors. The Lancet 355: 827-835.

Gubareva L.V. 2004. Molecular mechanisms of influenza virus resistance to neuraminidase inhibitors. Virus Research 103: 199-203.

Gürtler L. 2006. Virology of human influenza. In Kamps B.S., Hoffmann C., Preiser W. (eds), Influenza report 2006, 87-91. Paris : Flying Publisher, 2006.

Hirschfelder J., Stevenson D. and Eyring H. 1937. A theory of liquid structure. The Journal of Chemical Physics 5: 896-912.

Hinchliffe A. 2008. Molecular modelling for beginners. 2nd ed. Great Britain: John Wiley and Sons Ltd,

Fumio H. 2003. Molecular theory of solvation. Dordrecht: Spinger-Kluwer,

Hurt A.C., Lee R.T., Leang S.K., Cui L., Deng Y.M., Phuah S.P., Caldwell N., Freeman K., Komadina N., Smith D., Speers D., Kelso A., Lin R.T., Maurer-Stroh S.and Barr I.G.. 2011. Increased detection in Australia and Singapore of a novel influenza A(H1N1)2009 variant with reduced oseltamivir and zanamivir sensitivity due to a S247N neuraminidase mutation. Eurosurveillance 16 : 1-6.

Jackson D., Barclay W. and Zürcher T. 2005. Characterization of recombinant influenza B viruses with key neuraminidase inhibitor resistance mutations. Journal of Antimicrobial Chemotherapy 55: 162-169.

Jackson D., Elderfield R.A. and Barclay W.S. 2011. Molecular studies of influenza B virus in the reverse genetics era. Journal of General Virology 92: 1-17.

Janakiraman M.N., White C.L., Laver W.G., Air G.M. and Luo M. 1994. Structure of

influenza virus neuraminidase B/Lee/40 complexed with sialic acid and a dehydro analog at 1.8-A resolution: implications for the catalytic mechanism. Biochemistry 33: 8172-8179..

Jayaram B., Sprous D. and Beveridge D.L. 1998. Solvation Free Energy of Biomacromolecules: Parameters for a Modified Generalized Born Model Consistent with the AMBER Force Field. The Journal of Physical Chemistry B 102: 9571-9576.

Jorgensen W.L., Chandrasekhar J., Madura J.D., Impey R.W. and Klein M.L. 1983. Comparison of simple potential functions for simulating liquid water. The Journal of Chemical Physics 79: 926-935.

Karplus M. and McCammon J.A. 2002. Molecular dynamics simulations of biomolecules. Nature Structural Biology 9: 646-652.

Kawai N., Ikematsu H., Iwaki N., Satoh I., Kawashima T., Maeda T., Miyachi K., Hirotsu N., Shigematsu T. and Kashiwagi S. 2005. Factors Influencing the Effectiveness of Oseltamivir and Amantadine for the Treatment of Influenza: A Multicenter Study from Japan of the 2002—2003 Influenza Season. Clinical Infectious Diseases 40: 1309-1316.

Kiso M., Mitamura K., Sakai-Tagawa Y., Shiraishi K., Kawakami C., Kimura K., Hayden F.G., Sugaya N. and Kawaoka Y. 2004. Resistant influenza A viruses in children treated with oseltamivir: descriptive study. The Lancet 364: 759-765.

Kollman P.A., Massova I., Reyes C., Kuhn B., Huo S., Chong L., Lee M., Lee T., Duan Y., Wang W., Donini O., Cieplak P., Srinivasan J., Case D.A. and Cheatham T.E. 2000. Calculating Structures and Free Energies of Complex Molecules: Combining Molecular Mechanics and Continuum Models. Accounts of Chemical Research 33: 889-897.

Kovalenko A. and Hirata F. 1999. Potential of Mean Force between Two Molecular Ions in a Polar Molecular Solvent: A Study by the Three-Dimensional

Reference Interaction Site Model. The Journal of Physical Chemistry B 103: 7942-7957.

Kovalenko A. and Hirata F. 2000. Potentials of mean force of simple ions in ambient aqueous solution. I. Three-dimensional reference interaction site model approach. The Journal of Chemical Physics 112: 10391-10402.

Le Q.M., Kiso M., Someya K., Sakai Y.T., Nguyen T.H., Nguyen K.H.L., Pham N.D., Ngyen H.H., Yamada S., Muramoto Y., Horimoto T., Takada A., Goto H., Suzuki T., Suzuki Y. and Kawaoka Y. 2005. Avian flu: isolation of drug-resistant H5N1 virus. Nature 437: 1108-1108.

Lin Y.P., Gregory V., Bennett M. and Hay A. 2004. Recent changes among human influenza viruses. Virus Research 103: 47-52.

Malaisree M., Rungrotmongkol T., Decha P., Intharathep P., Aruksakunwong O. and Hannongbua S. 2008. Understanding of known drug-target interactions in the catalytic pocket of neuraminidase subtype N1. Proteins: Structure, Function, and Bioinformatics 71: 1908-1918.

Malaisree M., Rungrotmongkol T., Nunthaboot N., Aruksakunwong O., Intharathep P., Decha P., Sompornpisut P. and Hannongbua S. 2009. Source of oseltamivir resistance in avian influenza H5N1 virus with the H274Y mutation. Amino Acids 37: 725-732.

Massova I., and Kollman P.A. 2000. Drug Discovery and Design. Combined molecular mechanical and continuum solvent approach (MM-PBSA/GBSA) to predict ligand binding, 113–135. Netherlands : Kluwer Academic Publishers,

Matteoli E. and Mansoori G.A. 1995. A simple expression for radial distribution functions of pure fluids and mixtures. The Journal of Chemical Physics 103: 4672-4677.

Birnkrant D. and Cox E. 2009. The Emergency Use Authorization of Peramivir for Treatment of 2009 H1N1 Influenza. New England Journal of Medicine 361: 2204-2207.

Connolly M. 1983. Analytical molecular surface calculation. Journal of Applied Crystallography 16: 548-558.

Fogolari F., Brigo A. and Molinari H. 2002. The Poisson–Boltzmann equation for biomolecular electrostatics: a tool for structural biology. Journal of Molecular Recognition 15: 377-392.

Hatta M. and Kawaoka Y. 2003. The NB protein of influenza B virus is not necessary for virus replication in vitro. Journal of Virology 77 : 6050-6054.

Materials digital library pathway. Radial distribution function [online]. 2008. Available from: http://matdl.org/matdlwiki/index.php/softmatter:Radial_Distribution_Function [2012, April 12]

McKimm-Breschkin J.L. 2002. Neuraminidase inhibitors for the treatment and prevention of influenza. Expert Opinion on Pharmacotherapy 3: 103-112.

McQuarrie D.A.. 1976. Statistical Mechanics. New York : Harper and Row,

Mishin V.P., Hayden F.G. and Gubareva L.V. 2005. Susceptibilities of antiviral-resistant influenza viruses to novel neuraminidase inhibitors. Antimicrob Agents Chemother 49: 4515-4520.

Oakley A.J., Barrett S., Peat T.S., Newman J., Streltsov V.A., Waddington L., Saito T., Tashiro M. and McKimm-Breschkin J.L. 2010. Structural and functional basis of resistance to neuraminidase inhibitors of influenza B viruses. Journal of Medicinal Chemistry 53: 6421-6431.

Onufriev A., Bashford D. and Case D.A. 2004. Exploring protein native states and large-scale conformational changes with a modified generalized born model. Proteins: Structure, Function, and Bioinformatics 55: 383-394.

Pan D., Sun H., Bai C., Shen Y., Jin N., Liu H. and Yao X. 2011. Prediction of zanamivir efficiency over the possible 2009 Influenza A (H1N1) mutants by multiple molecular dynamics simulations and free energy calculations. Journal of Molecular Modeling. 17: 2465-2473.

Phongphanphanee S., Rungrotmongkol T., Yoshida N., Hannongbua S. and Hirata F. 2010. Proton Transport through the Influenza A M2 Channel: Three-Dimensional Reference Interaction Site Model Study. Journal of the American Chemical Society 132: 9782-9788.

Phongphanphanee S., Yoshida N. and Hirata F. 2008. On the Proton Exclusion of Aquaporins: A Statistical Mechanics Study. Journal of the American Chemical Society 130: 1540-1541.

Pinto L.H. and Lamb R.A. 2006. The M2 proton channels of influenza A and B viruses. Journal of Biological Chemistry 281: 8997-9000.

Rapaport D.C.. 2004. The art of molecular dynamics simulation. 2nd ed. England : Cambridge University Press,

Rungrotmongkol T., Malaisree M., Nunthaboot N., Sompornpisut P. and Hannongbua S. 2010a. Molecular prediction of oseltamivir efficiency against probable influenza A (H1N1-2009) mutants: molecular modeling approach. Amino Acids 39: 393-398.

Rungrotmongkol T., Nunthaboot N., Malaisree M., Kaiyawet N., Yotmanee P., Meeprasert A. and Hannongbua S. 2010b. Molecular insight into the specific binding of ADP-ribose to the nsP3 macro domains of chikungunya and venezuelan equine encephalitis viruses: Molecular dynamics simulations and free energy calculations. Journal of Molecular Graphics and Modelling 29: 347-353.

Rungrotmongkol T., Yotmanee P., Nunthaboot N and Hannongbua S. 2011. Computational studies of influenza A virus at three important targets:

hemagglutinin, neuraminidase and M2 protein. Current Pharmaceutical Design 17 : 1720-1739.

Russell R.J., Haire L.F., Stevens D.J., Collins P.J., Lin Y.P., Blackburn G.M., Hay A.J., Gamblin S.J. and Skehel J.J. 2006. The structure of H5N1 avian influenza neuraminidase suggests new opportunities for drug design. Nature 443: 45-49.

Ryckaert J.-P., Ciccotti G. and Berendsen H.J.C. 1977. Numerical integration of the cartesian equations of motion of a system with constraints: molecular dynamics of n-alkanes. Journal of Computational Physics 23: 327-341.

Sitkoff D., Sharp K.A. and Honig B. 1994. Accurate calculation of hydration free energies using macroscopic solvent models. The Journal of Physical Chemistry 98: 1978-1988.

Srinivasan J., Cheatham T.E., Cieplak P., Kollman P.A. and Case D.A.. 1998. Continuum solvent studies of the stability of DNA, RNA, and phosphoramidate-DNA helices. Journal of the American Chemical Society 120 : 9401–9409.

Still C., Tempczyk A., Hawley R. and Hendrickson T. 1990. Semianalytical treatment of solvation for molecular mechanics and dynamics. Journal of the American Chemical Society 112: 6127-6129.

Sugaya N., Mitamura K., Yamazaki M., Tamura D., Ichikawa M., Kimura K., Kawakami C., Kiso M., Ito M., Hatakeyama S. and Kawaoka Y. 2007. Lower clinical effectiveness of oseltamivir against influenza B contrasted with influenza A infection in children. Clinical Infectious Diseases 44: 197-202.

Taylor G. and Russell R. 2009. Influenza Virus Neuraminidase Inhibitors. In Bradshaw R.A. and Dennis E.A. (eds), Handbook of Cell Signaling, 2nd ed., 103-110. Elsevier Inc,

Treanor J.J. 2010. Influenza viruses, including avian influenza and swine influenza. In Mandell G.L., Bennett J.E. and Dolin R.D. (eds), Mandell, Douglas, and

Bennett's principles and practices of infectious diseases, 7th ed., 2265-2288. Philadelphia: Churchill Livingstone,

UDavis ChemWiki by University of California. Lennard-Jones potential [online]. 2012. Available from: http://chemwiki.ucdavis.edu/Physical_Chemistry/Quantum_Mechanics/Interm olecular_Forces/Lennard-Jones_Potential [2012, April 12]

Udommaneethanakit T., Rungrotmongkol T., Bren U., Frecer V. and Stanislav M. 2009. Dynamic behavior of avian influenza A virus neuraminidase subtype H5N1 in complex with oseltamivir, zanamivir, peramivir, and their phosphonate analogues. Journal of Chemical Information and Modeling 49: 2323-2332.

van der Vries E., Stelma F.F. and Boucher C.A.B. 2010. Emergence of a multidrug-resistant pandemic influenza A (H1N1) virus. New England Journal of Medicine 363: 1381-1382.

von Itzstein M. 2007. The war against influenza: discovery and development of sialidase inhibitors. Nat Rev Drug Discov 6: 967-974.

Ward P., Small I., Smith J., Suter P. and Dutkowski R. 2005. Oseltamivir (Tamiflu®) and its potential for use in the event of an influenza pandemic. Journal of Antimicrobial Chemotherapy 55: i5-i21.

Weiser J., Shenkin P.S. and Still W.C. 1999. Approximate atomic surfaces from linear combinations of pairwise overlaps (LCPO). Journal of Computational Chemistry 20: 217-230.

WHO. Flunet [online]. 2011. Available from: http://www.who.int/influenza/gisrs_laboratory/flunet [2012, February 28]

WHO. Influenza (Seasonal) [online]. 2009. Available from: http://www.who.int/mediacentre/factsheets/fs211 [2010, September 3]

Wikipedia. Accessible surface area [online]. 2012. Available from: http://en.wikipedia.org/wiki/Accessible_surface_area#cite_note-Shrake-1 [2012, April 12]

Wright P.F and Webster R.G. 2001. Orthomyxoviruses. In Knipe D.M., Howley P.M., Griffin D.E., Lamb R.A., Martin M.A., Roizman and Straus S.E. (eds), Fields virology, 4th ed., 1533–1579. Philadelphia : Lippincott Williams & Wilkins,

Yamashita M., Tomozawa T., Kakuta M., Tokumitsu A., Nasu H. and Kubo S. 2009. CS-8958, a Prodrug of the New Neuraminidase Inhibitor R-125489, Shows Long-Acting Anti-Influenza Virus Activity. Antimicrobial Agents and Chemotherapy 53: 186-192.

Yen H.-L., Ilyushina N.A., Salomon R., Hoffmann E., Webster R.G. and Govorkova E.A. 2007. Neuraminidase inhibitor-resistant recombinant A/Vietnam/1203/04 (H5N1) influenza viruses retain their replication efficiency and pathogenicity in vitro and in vivo. Journal of Virology 81: 12418-12426.

Yoshida N., Imai T., Phongphanphanee S., Kovalenko A. and Hirata F. 2008. Molecular recognition in biomolecules studied by statistical-mechanical integral-equation theory of liquids. The Journal of Physical Chemistry B 113: 873-886.

Zoete V., Meuwly M. and Karplus M. 2005. Study of the insulin dimerization: Binding free energy calculations and per-residue free energy decomposition. Proteins: Structure, Function, and Bioinformatics 61: 79-93.

# VITAE

| | |
|---|---|
| Name | Miss Jiraporn Tengrang |
| Date of birth | May 18, 1985 |
| Place of birth | Kantang, Trang, Thailand |
| Address | Department of Chemistry, Science, Chulalongkorn University |
| | Phayathai Road, Patumwan, Bangkok 10330, THAILAND |
| Telephone | +6622187602 |
| E-mail | jiraporn.te@gmail.com, Jiraporn.Te@Student.chula.ac.th |

**EDUCATIONS**

| | |
|---|---|
| 2009 – present | M.Sc. (Physical chemistry), Chulalongkorn University, Thailand |
| 2003 – 2007 | B.Sc. (2$^{nd}$ Class Honor, Chemistry), Prince of Songkla University, Thailand |